nature

https://doi.org/10.1038/s41586-025-09713-5

Accelerated Article Preview

Parity and lactation induce T cell mediated breast cancer protection

Received: 2 August 2024

Accepted: 6 October 2025

Accelerated Article Preview

Cite this article as: Virassamy, B. et al. Parity and lactation induce T cell mediated breast cancer protection. *Nature* https://doi.org/10.1038/s41586-025-09713-5 (2025)

Balaji Virassamy, Franco Caramia, Peter Savas, Michael A. Harris, Jia-Wern Pan, Jianan Wang, Emmaline Brown, Megan M. R. O'Malley, Courtney T. van Geelen, Michael Hun, Thomas N. Burn, Sneha Sant, Jamieson D. Ballan, Jasmine Kay, Luis E. Lara Gonzalez, Kylie Clarke, Han Xian Aw Yeang, Rejhan Idrizi, Metta Jana, Damon J. Challice, Roberto Salgado, Heather Thorne, kConFab consortium, Cathie Poliness, Sophie Nightingale, Soo-Hwang Teo, Terence P. Speed, Jane Visvader, Paul J. Neeson, Phillip K. Darcy, Laura K. Mackay & Sherene Loi

Parity and lactation induce T cell mediated breast cancer protection

Balaji Virassamy*[1,2], Franco Caramia*[1,2], Peter Savas*[1,2], Michael A Harris*[1,2], Jia-Wern Pan[3], Jianan Wang[1,2,], Emmaline Brown[1], Megan M. R. O'Malley[1,2], Courtney T van Geelen[1,2], Michael Hun[1,2], Thomas N Burn[4], Sneha Sant[1], Jamieson D Ballan[1,2], Jasmine Kay[1,2], Luis E Lara Gonzalez[1,2], Kylie Clarke[1], Han Xian Aw Yeang[1,2], Rejhan Idrizi[1,2], Metta Jana[1,2], Damon J Challice[1], Roberto Salgado[1,5], Heather Thorne[1,2], kConFab consortium[1*], Cathie Poliness[6], Sophie Nightingale[6], Soo-Hwang Teo[3], Terence P Speed[7], Jane Visvader[8,9], Paul J Neeson[1,2], Phillip K. Darcy[1,2], Laura K Mackay[#4] and Sherene Loi[#1,2]

Affiliations:

[1] Division of Cancer Research, Peter MacCallum Cancer Centre, Melbourne, Victoria, Australia.

[2] The Sir Peter MacCallum Department of Medical Oncology, University of Melbourne, Melbourne, Australia.

[3] Cancer Research Malaysia, Subang Jaya, Malaysia.

[4] Department of Microbiology and Immunology, The University of Melbourne at the Peter Doherty Institute for Infection and Immunity, Melbourne, Australia.

[5] GZA-ZNA Hospitals, Antwerp, Belgium.

[6] Department of Cancer Surgery, Peter MacCallum Cancer Centre, Melbourne, Australia.

[7] Department of Bioinformatics, the Walter and Eliza Hall Institute of Medical Research, Parkville, VIC 3052, Australia.

[8] Cancer Biology and Stem Cells Division, The Walter and Eliza Hall Institute of Medical Research, Parkville, VIC 3052, Australia.

[9] Department of Medical Biology, The University of Melbourne, VIC 3010, Australia.

* A list of the kConFab Investigators and their affiliations appears at the end of the paper.

* These authors contributed equally.

#Corresponding authors

Professor Sherene Loi, MD, PhD.

Peter MacCallum Cancer Centre, 305 Grattan St, Melbourne, AUSTRALIA 3000

Email:sherene.loi@petermac.org

Professor Laura K Mackay, PhD

Peter Doherty Institute for Infection and Immunity, Melbourne, AUSTRALIA 3000

Email: lkmackay@unimelb.edu.au

Abstract

Parity and breastfeeding reduce the risk of breast cancer, particularly triple-negative breast cancer (TNBC)[1,2], yet the immunological mechanisms underlying this protection remain unclear. Here, we show that parity induces an accumulation of $CD8^+$ T cells, including cells with a tissue-resident memory (T_{RM})-like phenotype within human normal breast tissue. In murine models, pregnancy followed by lactation and involution drove the accumulation of $CD8^+$ T cells in the mammary gland, coinciding with reduced tumour growth and increased intratumoural immune cell infiltration, effects that were abrogated by $CD8^+$ T cell depletion. Importantly, this $CD8^+$ T cell dependent tumour control was only observed following a complete cycle of lactation and involution. Consistent with this, primary TNBCs from parous women exhibited greater T cell infiltration and improved clinical outcomes. Together these findings, spanning preclinical models and over 1000 patient samples, provide new insight into how reproductive history shapes breast immunity, positioning $CD8^+$ T cells as key mediators of parity-associated protection and informing novel strategies for both prevention and treatment of breast cancer.

Key words:
Breast cancer prevention, Triple negative breast cancer, Pregnancy-associated breast cancer, Parity, Lactation and breastfeeding, $CD8^+$ Tissue-resident memory cells, Intratumoural $CD8^+$ T cells, Tumour infiltrating lymphocytes, Cancer immune surveillance.

Main

It is widely recognised that parity and lactation are associated with a reduced long-term risk of breast cancer[1,2]. Parity is thought to protect by reshaping mammary epithelial cell differentiation and growth pathways that occur during pregnancy, lactation, and involution, thereby reducing susceptibility to malignant transformation over time[3,4,5]. While parity has been associated with a decreased risk of hormone receptor-positive breast cancer, breastfeeding appears to confer a more specific reduction in the risk of triple-negative breast cancer (TNBC)[1,6]. The cellular and molecular mechanisms underlying this association are unclear. Deeper understanding could enable novel breast cancer subtype-specific prevention and treatment strategies. This could be particularly relevant for women at higher risk of TNBC, such as those who carry germline pathogenic variants, or for groups with poorer outcomes even after adjusting for key prognostic factors, such as certain ethnic groups[7].

The prognostic role of $CD8^+$ tumour infiltrating lymphocytes (TIL) is well established in both early and advanced stage TNBC[8,9] and T cell checkpoint inhibitors are now part of standard-of-care therapy, underscoring the critical role of host immunity. Our prior work demonstrated that a subset of $CD8^+$ T cells with a tissue-resident memory (T_{RM})-like phenotype mediates robust anti-tumour responses and is associated with reduced breast cancer recurrence[8,10]. We also showed that T_{RM}-like cells are present in both breast tumours and cancer-unaffected normal breast tissue, implicating them in treatment response and long-term immune surveillance of the breast.

Post-partum, immune cell populations in mammary tissue undergo considerable modulation: pregnancy and lactation are followed by widespread apoptosis and tissue remodelling in the process known as involution[11,12]. Changes in immune subsets, such as increased NKT T cells in the post-involution mammary gland, suggest a parity-induced immune surveillance mechanism[13]. Furthermore, circulating T cells increases in parous women have been observed to persist for months post-partum and are thought to contribute to autoimmunity[13-

[17]. Collectively, these observations suggest long-lasting immunologic breast remodelling after pregnancy, although the functional significance of these populations on tumour surveillance remains unclear. In this study, we tested the hypothesis that parity and post-lactational involution favourably reshape the mammary microenvironment by recruiting and retaining $CD8^+$ T cells that persist long term in the breast to enhance immune surveillance and protect against tumorigenesis.

Results

Parity associations with T cell quantity in human normal breast

To assess how reproductive history influences the immune landscape of normal breast tissue, we first compared the quantity and phenotype of $CD8^+$ T cells in cancer unaffected breast tissue from parous and nulliparous women[18]. We analysed single-cell (sc) transcriptomic data from four datasets comprising 985,662 single cells (including >35,000 $CD8^+$ T cells) from normal breast tissue of 170 adult women at average breast cancer risk, collated from Reed *et al*[15]. We observed that parous women (≥1 full-term pregnancy) had significantly higher proportions of $CD3^+$, $CD8^+$ and $CD8^+$ T_{RM}-like cells than nulliparous women (**Fig 1a**). Other immune subsets analysed did not differ significantly. (**Extended Data Fig 1a-e**).

We next evaluated immune infiltration by flow cytometry in cancer-unaffected healthy breast tissue from women undergoing prophylactic mastectomy including parous (n=65; >1 child) and nulliparous (n=25) individuals at high risk of breast cancer (**Sl. Table 1**). Compared to nulliparous women, breast tissue of parous women showed increased proportions of $CD45^+$, $CD3^+$ and $CD8^+$ lymphocytes and notably, significantly increased proportions of $CD8^+$ T cells expressing CD69 and CD103 canonical markers of tissue residency (T_{RM}-like cells, **Fig. 1b).** Multiplex OPAL staining further confirmed increased numbers of $CD3^+$, $CD8^+$, including a $CD69^+CD103^+CD8^+$ T_{RM}-like cell population in breast tissue from parous compared with

nulliparous women, with localisation predominantly in intraepithelial or periductal pan-cytokeratin positive regions (**Fig. 1c; Extended Data Fig. 2a,b)**. This dataset also allowed us to examine the long-term persistence of $CD8^+$ T_{RM}-like cells over a wide range of intervals between last live birth and tissue donation, in both pre- and post-menopausal women. $CD69^+CD103^+$ $CD8^+$ T cells were stably maintained for over 30 years after pregnancy and showed superior long-term retention compared with their $CD69^+CD103^-$ $CD8^+$ T cell counterparts, consistent with prior observations that $CD103^+$ T_{RM}-like cells predominate over time (**Fig. 1d)**[19,20].

To investigate the qualitative differences in breast-associated $CD8^+$ T cells related to parity and lactation, we performed bulk RNA-sequencing (RNA-seq) on T_{RM}-like cells isolated from breast tissue from parous cancer-unaffected women who had breast fed for ≥6 months, comparing gene expression profiles to autologous circulating $CD8^+$ T cells. We identified 347 differentially expressed genes in the parous breast T_{RM}-like cells (**SI. Table 2**), including upregulation of *ITGAE, ITGA1 and CXCR6*, hereafter called the "Parous breast-associated (PB)-T_{RM} signature" (**Fig 1e**). Analysis of an independent dataset comprising 109 normal breast tissue samples from cancer-unaffected women[21], revealed significant positive enrichment of the signature in parous compared to nulliparous women confirming parity-associated transcriptional differences (**Fig 1f**). We additionally confirmed that the PB-T_{RM} signature was significantly enriched in the $CD8^+$ T_{RM} compared with $CD8^+$ T_{EM} annotated single cells in the collated transcriptomic datasets[15] (**Extended Data Fig 2c**).

Lactation and involution enhance $CD8^+$ T cells in healthy murine MFP

We next investigated immune cell populations in the murine mammary fat pad (MFP) following pregnancy, lactation and involution in C57BL/6 mice under three conditions: (i) a complete cycle of natural lactation (21 days) followed by pup weaning, with tissue analysed at 28 days post-involution when the mammary gland had returned to a pre-pregnancy state (d28-inv) (ii) early force-weaned (FW) involution, where pups were removed within 12-24h of birth with

minimal lactation, with tissue analysed 10 days post-involution: d10-FW and (iii) age-matched controls to parous mice: virgin (**Fig. 2a**).

Immune profiling of the MFP at these timepoints revealed a selective increase in the frequency of $CD44^{hi}CD8^{+}$ T cells among $CD45^{+}$ populations in d28-inv mice (**Fig 2b, Extended Data Fig. 3a**). Total $CD45^{+}$ and $CD8^{+}$ T cell numbers were also significantly elevated compared to virgin mice, including $CD8^{+}$ T cell sub-populations expressing $CD69^{+}CD103^{-}$ and $CD69^{+}CD103^{+}$ (**Fig 2c, Extended Data Fig. 3b**). A similar enrichment of $CD8^{+}$ T cell subsets was observed in parous BALB/c mice at d28-inv, reinforcing this $CD8^{+}$ T cell response is a strain independent feature of the post-involution mammary gland (**Fig. 2d**). In contrast, $CD8^{+}$ T cells and T_{RM}-like cell populations were not significantly increased at d10-FW in C57BL/6 mice compared to virgin controls, and only modestly in BALB/c mice (**Fig. 2e, Extended Data Fig. 3c**). However, d10-FW mice did show a marked rise in ductal macrophages, consistent with previous reports[12,22] (**Fig. 2e**).

To further characterise parity-associated $CD8^{+}$ T cells, we next performed high-dimensional proteomic analyses. This revealed three clusters significantly enriched in d28-inv mice compared with virgin controls (**Fig. 2f**). All three clusters expressed canonical residency markers such as CD69, CD103 and CD49a along with differential expression of granzyme A, NK1.1 and CXCR3 (**Fig. 2g, Extended Data Fig. 4a**). Supporting the presence of T_{RM}-like cells, the d28-inv MFP also showed increased expression of *Tgfβ*2, *Tnf* and *Cxcl16* (**Extended Data Fig. 5a**), factors associated with $CD8^{+}$ T_{RM} development[23-25]. Consistent with our human breast tissue findings, OPAL fluorescence microscopy revealed a significant increase in $CD8^{+}$ T_{RM}-like cells in the MFP of d28-inv mice compared to virgin controls (**Extended Data Fig. 5b-d)**, with these cells located closer to E-cadherin^{+} epithelial cells (**Extended data Fig. 5e**). Together, these data show that a complete cycle of lactation and involution promotes the accumulation and epithelial association of $CD8^{+}$ T cells in murine mammary tissue, paralleling observations in the human normal breast.

Lactation and involution restrain murine mammary tumour growth

Accelerated tumour growth during early involution has been reported in preclinical models and associated with increased myeloid cell infiltration[11,26]. To further explore how different stages of involution affect tumour progression, we examined tumour growth in the MFP of d28-inv and d10-FW mice, compared to age-matched virgin controls using syngeneic orthotopic murine models of TNBC. To this end, AT3-OVA TNBC cells were injected into the MFP of C57BL/6 mice at the timepoints described above (**Fig. 2a**). Tumour growth in d10-FW mice was comparable to virgin controls (**Fig. 3a)**, consistent with previous reports[11]. In contrast, tumour growth was significantly reduced in d28-inv mice (**Fig. 3b**). This protective effect was also observed in BALB/c mice using the D2A1 BC cells, which lacks engineered antigens, such as ovalbumin (OVA), providing an additional model of parity-induced tumour suppression (**Fig 3c,d**).

Concomitant with reduced tumour outgrowth, we observed a significant increase in $CD8^+$ T cells in d28-inv AT3-OVA tumours compared to virgins (**Fig. 3e,f**) including OVA-specific tetramer$^+$ $CD8^+$ T cells and $CD69^+CD103^+$ T_{RM}-like subsets (**Fig. 3g**). Monocytes, $CD4^+$ Th1 cells, dendritic cells and $XCR1^+$ type I dendritic cells were also elevated in d28-inv tumours, while B cells, NK cells and T cell receptor (TCR)$\gamma\delta^+$ cells were not significantly changed (**Fig. 3g, Extended Data Fig. 6a**). In contrast, $CD8^+$ T cells were not increased in d10-FW AT3-OVA tumours compared to virgin controls (**Extended Data Fig. 6b**). Similarly, in D2A1 tumours, $CD45^+$ and $CD8^+$ T cell numbers were higher in d28-inv mice, but not in d10-FW mice, relative to virgin controls (**Extended Data Fig. 6c,d**).

$CD8^+$ T cells mediate parity-induced tumour protection

To investigate whether reduced tumour growth in parous mice was T cell-mediated, we inoculated virgin and d28-inv $RAG2^{-/-}\gamma c^{-/-}$ mice (lacking NK, T and B cells) with AT3-OVA cells and observed no difference in tumour growth (**Fig. 4a**). To assess whether $CD8^+$ T cells could

restore protection, we transferred naive $CD8^+$ TCR transgenic OT-I cells (specific for OVA) into $RAG2^{-/-}\gamma c^{-/-}$ mice prior to mating or into virgin controls. Tumour growth was significantly reduced in d28-inv compared with virgin mice (**Fig. 4b**), but not when tumour cells were inoculated at d10-FW (**Extended Data Fig. 7a**). Activated OT-I cells transferred prior to mating accumulated in greater numbers in the MFP at d28-inv compared to virgin mice (**Extended Data Fig. 7b**), indicating that the post-lactation mammary microenvironment promotes the differentiation of $CD8^+$ T_{RM}-like cells. In established tumours, $CD45^+$ and TCR-v$\alpha2^+$ $CD8^+$ T cells were elevated in d28-inv mice compared with virgins, but not in d10-FW (**Fig. 4c, Extended Data Fig. 7c**). Adoptive transfer of activated gBT-I cells (irrelevant specificity) into $RAG^{-/-}$ mice bearing AT3-OVA tumours had no effect on tumour growth (**Extended Data Fig. 7d**).

We next tested the requirement for $CD8^+$ T cells in parity-induced protection. For this, virgin and d28-inv mice were depleted of $CD8\alpha^+$, $CD8\beta^+$ or $CD4^+$ T cells before tumour inoculation and throughout the experiment (**Extended Data Fig. 8a-b**). As expected, isotype-treated d28-inv mice had lower tumour burdens than virgins, accompanied by increased $CD8\alpha^+CD44^{hi}$ T cell numbers in tumours (**Extended Data Fig. 8c,d**)**.** Critically, we found that tumour protection in d28-inv mice was significantly reduced by either CD8α or CD8β depletion alone, identifying $CD8\alpha\beta^+$ as the key mediators and excluding a dominant role for $CD8\alpha\alpha^+$ T cells (**Fig. 4d,e**). In virgins, only combined $CD8\alpha^+$ and $CD4^+$ T cell depletion increased tumour growth. Notably, $CD4^+$ T cell depletion alone enhanced tumour control in d28-inv mice. High dimensional proteomic analysis of $CD45^+$ cells from tumours revealed increased abundance of two clusters (C1 and C2) enriched for $CD8^+$ T cell and cDC1 markers in $CD4^+$ depleted d28-inv mice (**Extended Data Fig. 8e-k**).

To assess whether local $CD8^+$ T cells were sufficient for tumour control or whether circulating T cell recruitment was required, we treated virgin and d28-inv mice with the S1PR1 agonist FTY720 to block T cell egress before tumour inoculation (**Fig. 4f**). Tumour protection was lost in FTY720-treated d28-inv mice, accompanied by reduced tumour-specific $CD8^+$ T cells (**Fig**

4g-i). Collagen abundance did not differ in between virgin and d28-inv tumours (**Extended Data Fig. 8l,m)** suggesting that stromal differences are unlikely to explain T cell recruitment patterns. Together, these findings demonstrate that parity-induced tumour protection is mediated by conventional CD8αβ$^+$ T cells. Following lactation and involution, tumour challenge drives both expansion of the mammary-resident T cells and recruitment of circulating tumour-specific effectors, enhancing immune surveillance and tumour clearance.

Breastfeeding associated with immune infiltration in human TNBC

Having established that reduced tumour growth following lactation and involution in mice is dependent on CD8$^+$ T cells, we next asked whether a similar association exists in human TNBCs, where high T cell infiltrate is well known to correlate with improved prognoses[8]. Epidemiological studies also suggest that while parity may transiently increase breast cancer risk, breastfeeding attenuates the risk of developing TNBC[1]. To explore this, we examined the Malaysian MyBrCa cohort, which includes 934 women with early-stage breast cancer and detailed clinicopathologic and genomic information. We focused on the subset of 734 patients with recorded parity status and 656 with breastfeeding history[27,28]. In this cohort, the median maternal age at birth of first child was 27 years (range 14 – 43), the median number of children per woman was 3 (range 1-11) and the median lifetime breastfeeding duration in women who breastfed at all was 4 months (range 0.5 – 156, **SI. Table 3**). Using the gene expression derived ESTIMATE immune infiltrate score[29], our analysis revealed significantly higher tumoural immune content in basal-like (TNBC) in parous women overall, compared with the nulliparous women who subsequently developed breast cancer post-partum (**Fig. 5a)**. A similar increase in the ESTIMATE score was seen in parous women who breastfed compared to nulliparous women (**Fig 5b**). Additionally, we performed differential expression analysis between these “basal-like” tumours in parous versus nulliparous patients and parous-breastfeeding versus parous-non-breastfeeding patients. Moreover, the PB-T_{RM} signature generated in **Fig. 1f** was highly enriched with both parity and breastfeeding status (**Fig 5c,d**), highlighting the specificity of the PB-T_{RM} signature to breast involution by parity and lactation.

Furthermore, parous women who had breastfed had significantly greater intratumoural $CD8^+$ T cell density in basal-like tumours and when compared to other BC subtypes (**Fig 5e; Extended Data Fig. 9f**).

We further examined an independent of cohort of 270 Australian women who carry a germline pathogenic variant, who had been diagnosed with hormone receptor-negative early breast cancer after at least one full term pregnancy, with available breastfeeding history and survival outcomes (**Fig. 5f**, **SI. Table 4**). After adjustment for known prognostic factors, we found that patients who breastfed exhibited significantly longer overall survival (OS) after breast cancer diagnosis than patients who did not breastfeed (HR 0.39; 95%CI: 0.19, 0.79, p= 0.009; **Extended Data Fig 9a**). Using an established method to assess immune infiltration on haematoxylin and eosin-stained (H&E) digital slides[30], we found increased lymphocytic quantity in individuals with the longest breastfeeding duration (**Fig 5g**)**.** Although precise separation of parity and breastfeeding effects in human datasets is challenging, our analyses of two independent cohorts suggest that breastfeeding may contribute additional immune-mediated protection beyond parity alone.

To further support the general clinical relevance of the PB-T_{RM} signature, we examined associations with TILs and survival outcomes in the available early-stage breast cancer cohort[31,32]. We observed strong correlation of increased TIL quantities[30] with higher levels of the PB-T_{RM} signature in TNBC patients in the TCGA Breast Cancer dataset[32] (**Extended Data Fig 9b,c**). The PB-T_{RM} signature was also enriched in “basal-like” tumours and associated with improved disease specific and OS in the METABRIC dataset (**Extended Data Fig 9d,e**).

Discussion

The mammary gland undergoes profound structural and immunological changes across reproductive stages. While ductal macrophages in mammary gland biology are well studied, evidence increasingly supports a critical role for adaptive immunity, particularly during puberty and pregnancy[12,33]. Various immune cell subsets populate the ductal epithelium, and progesterone has been shown to influence T cell polarisation during pregnancy[11,33]. Additionally, breast cancers that develop in the immediate post-partum period have a poorer prognosis[34,35]. however, the mechanisms by which parity and breastfeeding confer long-term protection from TNBC have remained unclear.

We show that normal breast tissue from parous women harbours significantly more $CD8^+$ T cells, particularly those with a T_{RM}-like phenotype, compared to nulliparous women across diverse backgrounds[15]. Given $CD8^+$ T cell quantity is associated with improved TNBC outcomes, we hypothesised that parity-driven $CD8^+$ T cell responses could enhance long-term cancer immunosurveillance. Supporting this, $CD8^+$ T_{RM}-like cells in normal breast tissue from parous women were observed to persist for decades post-partum.

In murine models, completion of a full reproductive cycle was associated with reduced tumour growth and a sustained increase of T cells in the MFP, including those with a T_{RM}-like phenotype. These cells localised to the mammary epithelium under homeostatic conditions and were more frequently found within tumours following lactation, supporting their role in tumour immune surveillance. Depletion of conventional $CD8\alpha\beta^+$ T cells abrogated parity induced protection, confirming their essential functional role. Similarly, FTY720-mediated blockade of lymphocyte egress impaired tumour protection, suggesting that the parous mammary gland not only maintains resident $CD8^+$ T cells, but facilitates the recruitment of circulating tumour-reactive T cells from the periphery. This was accompanied by increased numbers of conventional type 1 dendritic cells the tumours of parous mice, consistent with enhanced $CD8^+$ T cell priming and maintenance[36]. Prior studies reporting expansion of

mammary intraepithelial lymphocytes and NKT cells via epithelial CD1d expression support the concept of immune remodelling after lactation, but our results indicate that these populations are not the primary mediators of tumour protection in our murine models[13,16,37]. Instead, our data complement these studies by demonstrating a durable, $CD8^+$ T cell-mediated layer of tumour protection in the mammary tissue post-lactation. These findings were paralleled in human TNBC, where tumours from parous women exhibited greater T cell infiltration, which also correlated with longer breastfeeding duration. Such associations may reflect cumulative antigen exposure, cytokine signalling or involution-associated tissue changes that promote long-term T cell retention.

Given known population-level variation in immune infiltration and breast cancer risk, it is important to consider how these findings may generalise across populations. For instance, higher TIL content in primary TNBCs from Asian compared to European populations has been previously reported, with exploratory sub-studies from phase III trials suggesting a numerically greater magnitude of benefit from checkpoint inhibition, though these comparisons remain hypothesis generating[38]. Although our findings focus on the potential preventive role of parity-induced $CD8^+$ T cells that are resident in the breast, they suggest that the immune contexture of the parous breast could influence TNBC therapeutic responsiveness. This is particularly relevant given the increasing use of immune checkpoint blockade in early-stage disease. However, we acknowledge that this remains the subject of future investigation.

Tumour-extrinsic factors, such as the mammary microbiome and dietary influences, may further modulate immune infiltration and tumour development[39]. Additionally post-partum tissue remodelling, including clearance of mutant clones and epigenetic changes[3,40] might act synergistically with $CD8^+$ T cell-mediated surveillance to eliminate premalignant cells. Similar immune-mediated protective mechanisms have been observed in other tissues, such as commensal skin human papilloma viruses promoting local $CD8^+$ T cell populations; immune mediated regression of early lung neoplastic conditions , HER2-specific T cells linked to parity-

associated protection of ductal carcinoma in situ (DCIS)[41-43]. These examples underscore the importance of physiological immune health in normal tissue as a mechanism for cancer prevention-- a concept we demonstrate here specifically for TNBC.

Our study has limitations. While we focused on TNBC, reproductive history might also influence immune mediated protection in other BC subtypes though this remains to be determined. We recognise that we did not assess hormone receptor-positive models due to limitations in preclinical systems, even though parity and breastfeeding is associated with reduced risk of all breast cancer subtypes. Oestrogen signalling has been shown to have diverse effects on immune cell function, with context and receptor-specific outcomes. While oestrogen can suppress certain immune responses via ERα signalling, ERβ activation in immune cells has been associated with enhanced anti-tumour activity[44]. Additionally, our human cohorts varied in reproductive histories, population backgrounds, time from tissue donation and last child, potentially introducing heterogeneity. Lastly, antigen specificity of the $CD8^+$ T cells identified remains undefined, warranting future research.

In conclusion, our findings reveal that lactation-associated remodelling of the mammary gland confers durable $CD8^+$ T cell-mediated protection against TNBC. By integrating data from murine models and diverse human populations, this work provides a new framework for understanding how reproductive history shapes long-term immune surveillance and influences breast cancer risk. These insights highlight the need for tailored prevention and treatment strategies that consider parity status and highlight the importance of systematically capturing reproductive history in future immunotherapy clinical trials- particularly critical given the rising global burden of breast cancer[45].

References

1. Jung, A.Y.*, et al.* Distinct Reproductive Risk Profiles for Intrinsic-Like Breast Cancer Subtypes: Pooled Analysis of Population-Based Studies. *J Natl Cancer Inst* **114**, 1706-1719 (2022).
2. Collaborative Group on Hormonal Factors in Breast, C. Breast cancer and breastfeeding: collaborative reanalysis of individual data from 47 epidemiological studies in 30 countries, including 50302 women with breast cancer and 96973 women without the disease. *Lancet* **360**, 187-195 (2002).
3. Feigman, M.J.*, et al.* Pregnancy reprograms the epigenome of mammary epithelial cells and blocks the development of premalignant lesions. *Nat Commun* **11**, 2649 (2020).
4. D'Cruz, C.M.*, et al.* Persistent parity-induced changes in growth factors, TGF-beta3, and differentiation in the rodent mammary gland. *Mol Endocrinol* **16**, 2034-2051 (2002).
5. Russo, J., Moral, R., Balogh, G.A., Mailo, D. & Russo, I.H. The protective role of pregnancy in breast cancer. *Breast Cancer Res* **7**, 131-142 (2005).
6. Islami, F.*, et al.* Breastfeeding and breast cancer risk by receptor status--a systematic review and meta-analysis. *Ann Oncol* **26**, 2398-2407 (2015).
7. Palmer, J.R.*, et al.* Parity, lactation, and breast cancer subtypes in African American women: results from the AMBER Consortium. *J Natl Cancer Inst* **106**(2014).
8. Harris, M.A.*, et al.* Towards targeting the breast cancer immune microenvironment. *Nat Rev Cancer* (2024).
9. Savas, P.*, et al.* Clinical relevance of host immunity in breast cancer: from TILs to the clinic. *Nat Rev Clin Oncol* **13**, 228-241 (2016).
10. Virassamy, B.*, et al.* Intratumoral CD8(+) T cells with a tissue-resident memory phenotype mediate local immunity and immune checkpoint responses in breast cancer. *Cancer Cell* **41**, 585-601.e588 (2023).
11. Hitchcock, J., Hughes, K., Pensa, S., Lloyd-Lewis, B. & Watson, C.J. The immune environment of the mammary gland fluctuates during post-lactational regression and correlates with tumour growth rate. *Development* **149**(2022).
12. Dawson, C.A.*, et al.* Tissue-resident ductal macrophages survey the mammary epithelium and facilitate tissue remodelling. *Nat Cell Biol* **22**, 546-558 (2020).
13. Hanasoge Somasundara, A.V.*, et al.* Parity-induced changes to mammary epithelial cells control NKT cell expansion and mammary oncogenesis. *Cell Rep* **37**, 110099 (2021).
14. Kumar, T.*, et al.* A spatially resolved single-cell genomic atlas of the adult human breast. *Nature* (2023).
15. Reed, A.D.*, et al.* A single-cell atlas enables mapping of homeostatic cellular shifts in the adult human breast. *Nat Genet* **56**, 652-662 (2024).
16. Corral, D.*, et al.* Mammary intraepithelial lymphocytes promote lactogenesis and offspring fitness. *Cell* **188**, 1662-1680.e1624 (2025).
17. Watanabe, M.*, et al.* Changes in T, B, and NK lymphocyte subsets during and after normal pregnancy. *Am J Reprod Immunol* **37**, 368-377 (1997).
18. Savas, P.*, et al.* Single-cell profiling of breast cancer T cells reveals a tissue-resident memory subset associated with improved prognosis. *Nat Med* **24**, 986-993 (2018).

19. Mackay, L.K., *et al.* Long-lived epithelial immunity by tissue-resident memory T (TRM) cells in the absence of persisting local antigen presentation. *Proc Natl Acad Sci U S A* **109**, 7037-7042 (2012).
20. Snyder, M.E., *et al.* Generation and persistence of human tissue-resident memory T cells in lung transplantation. *Sci Immunol* **4**(2019).
21. Santucci-Pereira, J., *et al.* Genomic signature of parity in the breast of premenopausal women. *Breast Cancer Res* **21**, 46 (2019).
22. Cansever, D., *et al.* Lactation-associated macrophages exist in murine mammary tissue and human milk. *Nat Immunol* **24**, 1098-1109 (2023).
23. Mackay, L.K., *et al.* T-box Transcription Factors Combine with the Cytokines TGF-beta and IL-15 to Control Tissue-Resident Memory T Cell Fate. *Immunity* **43**, 1101-1111 (2015).
24. Casey, K.A., *et al.* Antigen-independent differentiation and maintenance of effector-like resident memory T cells in tissues. *J Immunol* **188**, 4866-4875 (2012).
25. Di Pilato, M., *et al.* CXCR6 positions cytotoxic T cells to receive critical survival signals in the tumor microenvironment. *Cell* **184**, 4512-4530.e4522 (2021).
26. Martinson, H.A., Jindal, S., Durand-Rougely, C., Borges, V.F. & Schedin, P. Wound healing-like immune program facilitates postpartum mammary gland involution and tumor progression. *Int J Cancer* **136**, 1803-1813 (2015).
27. Pan, J.W., *et al.* The molecular landscape of Asian breast cancers reveals clinically relevant population-specific differences. *Nat Commun* **11**, 6433 (2020).
28. Pan, J.W., *et al.* Clustering of HR + /HER2- breast cancer in an Asian cohort is driven by immune phenotypes. *Breast Cancer Res* **26**, 67 (2024).
29. Yoshihara, K., *et al.* Inferring tumour purity and stromal and immune cell admixture from expression data. *Nat Commun* **4**, 2612 (2013).
30. Salgado, R., *et al.* The evaluation of tumor-infiltrating lymphocytes (TILs) in breast cancer: recommendations by an International TILs Working Group 2014. *Ann Oncol* **26**, 259-271 (2015).
31. Curtis, C., *et al.* The genomic and transcriptomic architecture of 2,000 breast tumours reveals novel subgroups. *Nature* **486**, 346-352 (2012).
32. Liu, J., *et al.* An Integrated TCGA Pan-Cancer Clinical Data Resource to Drive High-Quality Survival Outcome Analytics. *Cell* **173**, 400-416.e411 (2018).
33. Plaks, V., *et al.* Adaptive Immune Regulation of Mammary Postnatal Organogenesis. *Dev Cell* **34**, 493-504 (2015).
34. Galati, F., *et al.* Pregnancy-Associated Breast Cancer: A Diagnostic and Therapeutic Challenge. *Diagnostics (Basel)* **13**(2023).
35. Amant, F., *et al.* The definition of pregnancy-associated breast cancer is outdated and should no longer be used. *Lancet Oncol* **22**, 753-754 (2021).
36. Murphy, T.L. & Murphy, K.M. Dendritic cells in cancer immunology. *Cell Mol Immunol* **19**, 3-13 (2022).
37. Jaquish, A., *et al.* Mammary intraepithelial lymphocytes and intestinal inputs shape T cell dynamics in lactogenesis. *Nat Immunol* **26**, 1411-1422 (2025).
38. Im, S.A., *et al.* Results from the randomized KEYNOTE-355 study of pembrolizumab plus chemotherapy for Asian patients with advanced TNBC. *NPJ Breast Cancer* **10**, 79 (2024).

39. Wang, H.*, et al.* The microbial metabolite trimethylamine N-oxide promotes antitumor immunity in triple-negative breast cancer. *Cell Metab* **34**, 581-594.e588 (2022).
40. Cereser, B.*, et al.* The mutational landscape of the adult healthy parous and nulliparous human breast. *Nat Commun* **14**, 5136 (2023).
41. Lowenfeld, L.*, et al.* Dendritic Cell Vaccination Enhances Immune Responses and Induces Regression of HER2pos DCIS Independent of Route: Results of Randomized Selection Design Trial. *Clinical Cancer Research* **23**, 2961-2971 (2017).
42. Strickley, J.D.*, et al.* Immunity to commensal papillomaviruses protects against skin cancer. *Nature* **575**, 519-522 (2019).
43. Datta, J.*, et al.* Progressive loss of anti-HER2 CD4(+) T-helper type 1 response in breast tumorigenesis and the potential for immune restoration. *Oncoimmunology* **4**, e1022301 (2015).
44. Chakraborty, B.*, et al.* Estrogen Receptor Signaling in the Immune System. *Endocr Rev* **44**, 117-141 (2023).
45. Coles, C.E.*, et al.* The Lancet Breast Cancer Commission. *Lancet* **403**, 1895-1950 (2024).

Main Figure Legends

Figure 1. Parity is associated with a significantly increased T cells in cancer unaffected human breast.

a. Immune cell abundance in normal breast from scRNAseq (Y-axes: cell type frequency) calculated by indicate immune cells over total epithelial cells in average BC risk women (n=170). Violin plots show data distribution with boxplots indicate IQR (Interquartile range) extension from Q1 to Q3 and median as a white bar, whiskers extend to the most extreme dot point within 1.5xIQR, and points beyond show outliers. Two-sided Wilcoxon rank sum test, unadjusted p-value shown; total cells=985,662; $CD45^+$=120,467 from nulliparous (N, n=53) vs parous (P, n=117). CD3+ (n=72,288 cells) in (N, n=53) vs (P, n=115). $CD8^+$ (n=38,834cells) in (N, n=53) vs (P, n=114) and $CD8^+$ T_{RM} (n=18,963 cells) in (N, n=53) vs (P, n=114). **b.** Proportions of $CD45^+$, $CD3^+$, $CD8^+$ T cells over total cells and $CD69^+CD103^-$ and $CD69^+CD103^+$ T cells over total $CD45RA^-CCR7^-CD8^+$ T cells (Y-axes) by flow cytometry (N; n=25) and (P; n=65) normal breast in high BC risk women. (N vs P defined as 1 or more full-term pregnancies); refer to methods for further details; two-sided Wilcoxon rank-sum test, unadjusted for multiple comparisons. **c.** Representative OPAL images of N vs P normal breast stained for DAPI, (AE1/AE3), CD3, CD8, CD69, and CD103. Green indicates representative $CD8^+$ and white indicates merged $CD69^+CD103^+CD8^+CD3^+$ T cell; refer to methods for further details **d.** Persistence of $CD69^+CD103^-$ vs $CD69^+CD103^+CD8^+$ T cells over time (X-axis) years from last live birth to human breast donation (n=65). Datapoints coloured according to age <50 or >50 for menopausal status. Unadjusted two-sided p value. **e.** Volcano plot of breast $CD69^+CD103^+CD8^+$ vs autologous circulating $CD8^+$ T cells from non-cancerous parous women (n=3). Significantly upregulated genes in $CD69^+CD103^+CD8^+$ (limma test, FDR<1%, logFC>1): referred as parous breast (PB)-T_{RM} signature, **f.** GSEA of PB-T_{RM} signature from normal breast 109) women (N, n=30 vs P, n=79) from Santucci *et al*[21]. Exact p values are shown.

Figure 2: Complete lactation and involution significantly increased CD8⁺ T cells in healthy murine mammary tissue.

a. Experimental schema of parity **b.** Donut plots indicating immune cell frequency among $CD45^+$ cells in the mammary fat pad (MFP) analysed by flow cytometry from virgin (n=9) and d28-inv (n=12) C57BL/6 healthy mice, highlighting the $CD8\alpha^+CD44^{hi}$T cells in green colour. **c.** Number of indicated immune cell sub-populations per gram of MFP from virgin (n=9) and d28-inv (n=12) C57BL/6 mice. **d.** Number of indicated immune cell sub-populations per gram of MFP from virgin (n=8) and d28-inv (n=8) BALB/c mice. **e.** Number of indicated immune cell sub-populations per gram of MFP from virgin (n=8) and d10-FW (n=8) C57BL/6 mice. **f.** UMAP of $CD8\alpha^+$ T cells generated from flow cytometry data from the MFP of C57BL/6 virgin (n=8) and d28-inv (n=9) mice with three enriched clusters indicated. Each dot represents an individual cell. **g.** Feature plots of indicated markers on $CD8\alpha^+$ T cells projected on UMAP. Data in graphs represent mean ±SEM, results represent two combined biologically independent experiments. Statistical significance determined by two-sided (c-e) or one sided (f) Mann-Whitney test. Exact p values are shown or $p < 0.0001$ in instances where p values are extremely small.

Figure 3: Lactation and involution restrain tumour growth and is significantly associated with increased murine mammary CD8⁺ TILs

a. Tumour growth (left) curves and endpoint tumour volume (right) of AT3-OVA TNBC cells injected into the 4^{th} MFP of in d10-FW (n=7) and age-matched virgin control (n=7) C57BL/6 mice. **b.** Tumour growth (left) and endpoint tumour volume (right) of AT3-OVA cells in d28-inv (n=8) and age-matched virgin control (n=8) C57BL/6 mice. **c.** Tumour growth (left) and endpoint tumour volume (right) of D2A1 cells injected into d10-FW (n=9) and age-matched virgin control BALB/c mice (n=10). **d.** Tumour growth (left) of D2A1 cells in d28-inv (n=10) and age-matched virgin (n=11) control mice and endpoint tumour volume (right) of d28-inv (n=5) and age-matched virgin (n=6) BALB/c mice. **e.** Donut plot of immune cell frequency analysed

by flow cytometry among all CD45$^+$ cells in AT3-OVA tumours from virgin (n=9) and d28-inv (n=10) mice 23-25 days post BC tumour cell injection. **f.** Ratio of CD8$^+$ to CD4$^+$ T cells and frequency of CD8$^+$ T cells among all CD45$^+$ cells AT3-OVA tumours from virgin (n=9) and d28-inv (n=10) mice. **g.** Numbers of indicated immune cell sub-populations per gram of AT3-OVA tumour from virgin (n=9) and d28-inv (n=10) C57BL/6 mice. Data in graphs represent mean ±SEM, results represent two combined independent experiments. Statistical significance determined by two-sided Mann-Whitney test. Exact p values are shown or p < 0.0001 in instances where p values are extremely small.

Figure 4: Parity induced protection against breast cancer is mediated by CD8$^+$ T cells

a. AT3-OVA tumour growth (left) and endpoint tumour burden (right) in the 4th MFP of RAG2$^{-/-}$γc$^{-/-}$ mice in d28-inv (n=13) and age-matched virgin controls (n=14). **b.** AT3-OVA tumour growth (left) and endpoint tumour burden (right) in the 4th MFP of RAG2$^{-/-}$γc$^{-/-}$ mice pre-inoculated with OT-I cells seven days prior to mating in d28-inv (n=11) and matched controls (n=10). **c.** Numbers of indicated immune cells per gram of AT3-OVA tumour from virgin (n=6) and d28-inv (n=6) RAG2$^{-/-}$γc$^{-/-}$ mice at four weeks post tumour development. **d.** AT3-OVA tumour growth in the 4th MFP of C57BL/6 mice in virgin (left) and d28-inv (right) mice treated with anti-CD4 (virgin n=12; d28-inv n=13), anti-CD8α (n=9), anti-CD8β (virgin n=12; d28-inv n=14), and combined anti-CD4/CD8α (n=14) or isotype control (n=16). **e.** Endpoint AT3-OVA tumour weight of AT3-OVA of C57BL/6 mice in virgin (left) and d28-inv (right) mice depleted with anti-CD4 (virgin n=12; d28-inv n=13), anti-CD8α (n=9), anti-CD8β (virgin n=12; d28-inv n=14), and combined anti-CD4/CD8α (n=14) or isotype control (n=16). **f.** Number of CD3$^+$ T cells per ul blood in virgin and d28-inv C57BL/6 mice treated with FTY720 (n=8) or vehicle (n=8). **g.** AT3-OVA tumour growth post FTY720 treatment in the indicated time points (virgin n=11; d28-inv n=15) or vehicle (virgin n=12; d28-inv n=15). **h.** Endpoint AT3-OVA tumour weight in virgin and d28-inv C57BL/6 mice treated with FTY720 (virgin n=11; d28-inv n=15) or vehicle (virgin n=12; d28-inv n=15). **i.** Number of OVA-tetramer$^+$ T cells per gram of AT3-OVA

tumour (virgin n=10; d28-inv n=13) or vehicle (virgin n=10; d28-inv n=15) analysed 23-25 days post treatment. Data in graphs represent mean ±SEM from two combined independent experiments. Two-sided Mann-Whitney test (a-c), Two-Way ANOVA at endpoint (d,g), Kruskal-Wallis (f,i) or One-Way ANOVA. Exact p values are shown or $p < 0.0001$ in instances where p values are extremely small.

Figure 5: Parity and breastfeeding are associated with increased TILs in women with primary TNBC.

a. Effect of parity on subsequent tumour immune infiltration calculated with RNASeq based (ESTIMATE) score in MyBrCa cohort. Linear model for ESTIMATE score with parity and sequencing batch as covariates. β is the estimated non-standardised coefficient for parity with 95% CI. **b.** Immune (ESTIMATE) score from MyBrCa with known breastfeeding (BF) status prior to BC. ANOVA with breastfeeding status and sequencing batch as covariates; two-sided, 95% CI, mean difference shown by Tukey's HSD test. p values adjusted for intra-subtype comparisons only. **c.** GSEA of the PB-T_{RM} signature in parous vs nulliparous women in the MyBrCa basal cohort. **d.** GSEA of the PB-T_{RM} signature in breastfed compared to non-breastfed (no-BF) parous women in MyBrCa basal cohort. **e.** Intratumoural T cell density in Basal-like BC determined by immunohistochemistry for $CD8^+$ and $CD3^+$ in MyBrCa, comparing N vs P women by breastfeeding durations prior to BC. Percent $CD8^+$ and $CD3^+$ T cell density quantified as ratio of stain-positive pixels to all pixels within tumour margins. Modelled with β-regression adjusting for covariates of age at diagnosis and tumour grade. Presented unadjusted p values with average marginal effect (AME) for each group compared to N. **f.** Kaplan–Meier survival analysis of overall survival in women (n = 270) diagnosed post-partum with primary hormone receptor-negative BC, stratified by breastfeeding status (Yes vs No). Univariate Cox regression hazard ratio with 95% CI. **g.** Quantity of stromal tumour infiltrating lymphocytes (TIL) quantified on standard H&E-stained digital slides from primary hormone receptor–negative high familial risk women (n=136). Age-adjusted percentage

infiltration (y-axis) by breastfeeding duration (x-axis; **SI. Table 4**). Horizontal lines indicate medians, vertical lines the IQR. Group differences tested with Kruskal–Wallis. (a,b,e) box plots horizontal bar shows median, hinges represent IQR and whiskers extend to the most extreme dot point within 1.5xIQR, and points beyond show outliers. Exact p values are shown.

Methods

Patient samples

This project was approved by the Human Research Ethics Committee of the Peter MacCallum Cancer Centre (project approval number "SEGMENT" 13/123 and 97/27 for the Kathleen Cuningham Foundation Consortium for Research into Familial Breast Cancer (kConFab) with project approval numbers #129 and #150). All participants provided written informed consent prior to tissue and blood collections. Ethics approvals for the human MyBrCa cohort can be found in the originating publication Pan *et al* 2024.

Tissue processing of Human Normal Breast

Cancer-unaffected normal breast tissues were collected from prophylactic mastectomies from women from high-risk familial cancer families. Mammary tissues were divided into segments and either placed in neutral buffered formalin for processing to formalin fixed paraffin embedded blocks, or a single cell suspension was created for further processing. Briefly, adipose tissue was removed from mammary glands and the associated connective tissues were then finely diced into smaller fragments in RPMI1640 containing, 1 mg/ml collagenase type 4 (Worthington biochemical, Lakewood, NJ), 30U/ml DNase (Roche diagnostics, Indianapolis, IN, USA) and incubated for 30 minutes at 37^0C. Digested tissue fragments were teased through a 70-um sterile cell strainer, the sieve irrigated with Dulbecco's phosphate-buffered saline (PBS) and the homogenised cells collected into multiple 50ml conical tube. Pelleted cells were stained with monoclonal antibodies for immunophenotyping and resuspended in 2% paraformaldehyde (PFA) buffer for flow cytometric spectral analysis.

Antibody labelling human cells for FACS

Homogenised cells in suspension were labelled with monoclonal antibodies for 30 minutes at 4^0C in FACS buffer (2% fetal bovine serum in Dulbecco's PBS), washed twice in FACS wash buffer. Antibody panel included CD45 and HLA-ABC to discriminate lymphocytes from other

stromal and epithelial cell compartments in suspension, T cell markers CD3, CD4 and CD8, the T cell differentiation markers CCR7, CD45RA, CD69 and CD103. Viable cells were revealed using the fixable zombie red, PE-Tex-red or fixable yellow viability dyes (Biolegend, San Diego, CA). Compensation controls were prepared for each antibody using UltraComp beads (BD Biosciences, San Diego, CA, USA). Multi-parameter flow cytometry data was acquired on the BD FACS Symphony A5 or LSR Fortessa X-20 instrument (BD Biosciences, San Diego, CA, USA) and data analysed using FlowJo v10 (BD Biosciences, San Diego, CA, USA). A representative flow cytometry gating strategy of immune cells in human normal breast tissue is shown in **Extended data Figure 10a.**

Human normal breast data analysis

Two-sided Wilcoxon rank-sum tests were used to compare parous and nulliparous groups across different T cell sub-populations. beta regression was used to model the interval from last birth to tissue donation and how this affected $CD8^{+}CD103^{-}$ and $CD8^{+}CD103^{+}$ T cells, as implemented in the betareg R package (v3.2-1). Regression lines fitted using beta regression, controlling for age at tissue donation, with 95% confidence intervals shaded. Average Marginal Effect (AME) for trend over time, representing change in % abundance per 1 year increase in birth to donation interval (**Main Fig. 1d**). Age at tissue donation was included as a continuous covariate. The AME of the interval since last pregnancy was estimated using the 'margins' function from the margins R package (v0.3.28), interpreted as the average change in cell proportion per year increase in the interval, averaged over the empirical distribution of age at tissue donation. To represent model fit on plot and calculate confidence intervals, the fitted beta regression model was supplied to the 'ggpredict' function of the ggeffects R package (v2.2.1).

Murine tissue processing and FACS

Spleens were mashed through a 70-um cell strainer and incubated with red cell lysis buffer for 5 minutes are room temperature prior to staining. Murine mammary tissue with lymph nodes

removed or tumour were minced into fragments and incubated in RPMI1640 containing, 1 mg/ml collagenase type 4 and DNAse II at 0.2 mg/mL for 30 minutes at 37^{o}C with shaking (300 rpm). Cells were serially passed and washed through 70-um strainers followed by viability staining in PBS then FcR blockade (2.4G2) at 1:500 dilution for 10 minutes at room temperature and prior to FACS staining with surface FACS antibodies in FACS wash buffer (4% FCS, 2 mM EDTA) containing BD Horizon Brilliant Stain Buffer Plus (BD). Post staining with antibody cocktail for 30 minutes at room temperature, samples were washed twice with FACS wash buffer and fixed with Foxp3/Transcription Factor Staining Buffer Set (Invitrogen) as per the manufacturer's instructions. Samples were either resuspended in 2% PFA or underwent intracellular staining in Foxp3/Transcription Factor permeabilization buffer followed for 30 minutes at room temperature. Intracellular stained samples were washed twice and resuspend in 2% PFA. Samples were analysed on a BD Symphony FACS analyser or 5-laser Cytek Aurora. Data was analysed using FlowJo v10 or OMIQ cloud-based platform.

OMIQ was used for high dimensional analysis. Data was scaled using hyperbolic arcsine (asinh) transformation and clustered using Phenograph. For high dimensional analysis of immune cells in the mammary fat pad TCR$\gamma\delta^{+}$ and CD1d^{+} cells were excluded and CD45^{+} TCRβ^{+} CD8α^{+} cells were clustered based on the expression of Granzyme B, CD38, CD62L, TCF-1, CD49a, NK.1, CD8β, Slamf6, CD103, CD44, Ly6C, KLRG1, CXCR3, CD39, PD1, CD244, Tbet, CD69, CXCR6, CD8α and Granzyme A. For high dimensional analysis of immune cells in AT3-OVA tumours CD45^{+} cells were clustered based on the expression of CD19, NK1.1, CD3, TCRb, TCR$\gamma\delta$, CD8α, CD8β, CD4, CD44, CD62L, CD69, CD103, CD49a, CD11b, CD11c, F480, MHC-II, Siglec-F, XCR1, SIRPα, CX3CR1, CD64, CD39, OVA-tetramer, PD-1, PD-L1, LAG3, KLRG1, CD38, FOXP3, Tbet, TCF-1, CTLA-4.

Bulk RNAseq gene expression analysis

Cancer unaffected normal breast tissue associated CD69^{+}CD103^{+}CD8^{+} T cells and autologous blood derived CD8^{+} circulating T cells (5x10^{3}-1x10^{4} cells) were FACS purified, BD

FACSAria II Cell Sorter (BD Biosciences). Reanalysis of isolated $CD8^+$ T cell sub-populations following FACS were assessed for >90% purity of individual samples. Total RNA was extracted from indicated T cell sub-populations from n=3 pooled cancer unaffected normal breast tissue using the RNeasy mini kit (Qiagen, Netherlands) as per the manufacturer's instructions. RNA Tape Station (Agilent, USA) analysis was performed as per the manufacturer's instructions to assess the quantity and quality of RNA present in the sample. 2-5 ng used for RNA library preparation according to the manufacturer's instructions with ribo-depletion NEB. The library was then amplified with 3' PCR primers containing sample indices and the Illumina clustering guides. 10X lysis Buffer is a cell lysis buffer that can be used together with the SMARTer Ultra Low Input RNA Kit for Sequencing v3 and the SMART-Seq v4 Ultra Low Input RNA Kit for Sequencing. Indexed libraries were pooled and sequenced on Illumina NextSeq HO 75SE (Illumina). Two to five million single-end reads were generated as an output. Adaptor trimming was performed, and reads were aligned to the mm10 reference genome using HISAT2 (v2.2)[46]. Aligned reads were quantified using HTSeq (v2.0.3). Counts were normalised and unwanted variance introduced by library size differences was removed using RUV-III (v0.9.7.1) in R. Differential expression analysis was performed using limma (v3.60.3). Volcano plots were produced with custom code with ggplot2 (v3.5.1). The PB-T_{RM} signature derived from differential expression analysis by filtering the genes by FDR<1% and logFC>1. A gene expression dataset of pre-menopausal parous and nulliparous human breast tissue was accessed GEO: GSE112825 We used limma[47] to analyse the previously normalised expression and perform differential expression analysis of parous against nulliparous women. To detect enrichment of our derived PB-T_{RM} gene signature, we performed gene set enrichment analysis (GSEA) using the differential expression results with the fgsea (v1.30.0) library in R (v4.4.1)[48].

Single cell cohort from Reed *et al.*

The processed and annotated single cell normal breast tissue atlas presented by Reed *et al* 2024 was used, only cells annotated as "not sorted" or "live sorted" were collated from several

different datasets of normal human breast tissue. We used samples from women annotated as “average risk” or “unknown risk” of breast cancer- i.e. normal breast samples from reduction mammoplasties and not cancer mastectomies or prophylactic mastectomies and where parity status was known.

To calculate and compare abundance of normal breast cell types between parous and nulliparous women, we calculated ratios of $CD3^+$T cells, $CD8^+$ T cells and $CD8^+$ T_{RM}-like cells over total epithelial cells per sample compared using unpaired Wilcoxon test and shown Violin plots produced in R (v4.4.1). We conducted a focused analysis on the $CD8^+$ T cells performing integration with Harmony (v1.2.3)[49] using default parameters (using dataset and donor as covariates), dimensionality reduction and visualisation with Seurat (v5.2.1)[50]. We used the scaled gene counts and calculated single cell signature enrichment of the PB-T_{RM} signature using the AUCell (v1.28.0) package in R[51]. We compared single cell enrichments of two different previously annotated $CD8^+$ T cell sub-populations ($T_{EM\ and}$ T_{RM}-like) using the unpaired Wilcoxon rank-sum test.

Murine cell lines

AT3-OVA cells were provided by Prof. Phil Darcy (Peter MacCallum Cancer Centre, Melbourne, VIC, Australia). D2A1 cells[52] were provided by A/Prof. Kara Britt (Peter MacCallum Cancer Centre, Melbourne, VIC, Australia). AT3-OVA TNBC cells were generated by transducing the parental AT3 cell line with a retroviral vector pMIG/MSCV-IRES-eGFP plasmid encoding membrane-bound chicken ovalbumin (OVA) cDNA (model antigen) protein, tagged with GFP as previously described[53]. Both cell lines were well established from Peter MacCallum Cancer Centre laboratory stocks and published. Breast cancer cells were cultured with complete DMEM media supplemented with 10% FCS. For *in vivo* experiments, $2.5x10^5$ AT3-OVA or $1x10^4$ D2A1 cells at an early passage state were resuspended in 50 µL phosphate buffer saline (PBS) solution at neutral pH and injected orthotopically into the right 4^{th} mammary fat pad (MFP) of mice. Cell lines were verified to be mycoplasma negative at the Victorian

Infectious Diseases References Lab (Melbourne, VIC, Australia) and were maintained at 37ºC in a humidified incubator at 5% CO_2.

Mouse tumour and parity models

All animal experiments conducted in this study were approved by the relevant Peter MacCallum Cancer Centre Animal Experimentation Ethics Committee (E648, 2025-05) or by The University of Melbourne Animal Ethics Committee (21938) and conducted in accordance with the National Health and Medical Research Council Australian Code of Practice for the Care and Use of Animals for Scientific Purposes.

C57BL/6J wild type (wt), BALB/c wt, RAG2$^{-/-}$γc$^{-/-}$, RAG1$^{-/-}$, gBT-I and OT-I CD45.2 wt female mice were obtained from the Walter and Eliza Hall Institute of Medical Research or bred in-house (VIC, Australia). Mice were allocated to experiments at 7-8 weeks of age. For tumour models, volume (length x width^2 x 0.5) was calculated by vernier caliper following development of palpable tumours and measurements were taken every 3-4 days. Mice were euthanised when MFP tumours reached an ethical limit of up to 1500 mm^3, or if the animals showed any signs of adverse health indications as per Peter MacCallum cancer center institutional guidelines. For parity experiments, dams were whitened prior to the introduction of stud males to establish breeding pairs/trios. Pregnancy was confirmed by plug formation and studs removed. After littering, dams underwent complete lactation and with pups for 21 days and for forced wean experiments pups were removed at birth within 12-24 hours from the dams post-partum and sacrificed (“d10-FW” timepoints). Dams that underwent early pup-removal were immediately co-housed with other female mice and did not exhibit changes in social behavior, housing conditions for the mice were followed as per institutional guidelines, including dark/light cycle, ambient temperature and humidity conditions.

Adoptive transfer of transgenic T cells

OT-I cells were isolated utilising the negative immunomagnetic cell separation method, MACS (Stem cell Technologies, Vancouver, BC) from the spleen of wildtype OT-I CD45.2 donor mice. A total of 2.5 x 10^5 OT-I cells were intravenously transferred to recipient RAG2$^{-/-}$γc$^{-/-}$ mice, seven days before mating and in house breeding began. OT-I cells were immunophenotyped by flow cytometry to assess the purity of OT-I cell isolation (>90-95%) with the use of CD45.2, TCR-vα2, CD8α, CD44 and CD62L cell surface markers. For experiments with effector OT-I cells, T cells were activated in culture for 4 days with $OVA_{257-264}$ (SIINFEKL) peptide-pulsed, irradiated (50Gy) splenocytes in the presence of recombinant human IL-2 (25U ml^{-1}; PeproTech) at 37^{o}C and 5% CO_2 and 1 x 10^4 were injected intravenously (i.v.) per mouse.

For the gBT-I experiment HSV-specific gBT-I transgenic T cells were activated in culture for 4 days with $gB_{498-505}$ (SSIEFARL) peptide-pulsed, irradiated (50Gy) splenocytes in the presence of recombinant human IL-2 (25U ml^{-1}; PeproTech) at 37^{o}C and 5% CO_2. 20x10^6 activated gBT-I cells were injected i.v. into naïve Rag1$^{-/-}$ mice. 56-62 days following gBT-I cell transfer, mice were subsequently inoculated orthotopically with 5x10^5 AT3-OVA cells into the 4th MFP as described above.

T cell depletion experiments

C57BL/6 mice were mated as described above prior to being allocated to tumour experiments. Seven days prior to AT3-OVA tumour challenge nonrandomised mice were injected intraperitoneally (i.p.) with 200 µg IgG2 isotype control combined with 200 µg anti-CD4 (Clone GK1.5, Bio X Cell Leganon, USA) anti-CD8α (Clone YTS, Bio X Cell,) anti-CD8b (Clone 53-5.8, Bio X Cell,) or 400 µg IgG2 isotype control (Bio X Cell) twice then once weekly.

Fingolimod (FTY720) *in vivo* treatments

C57BL/6 mice were mated as described above prior to being allocated to tumour experiments.. Briefly, three days prior to AT3-OVA challenge mice were injected i.p. with 1 mg/kg FTY720 compound reconstituted in 2% 2-hydroxypropyl-beta-cyclodextrin (Merck) or vehicle control

(2% 2-hydroxypropyl-beta-cyclodextrin) with daily injections separated by one day breaks every five days.

Murine histology and OPAL analysis

Intact 4th mammary fat pad of C57BL/6 mice were fixed in 10% neutral buffered formalin for 24 hours and then processed and embedded into formalin-fixed paraffin embedded (FFPE) blocks. 4-µm-thick sections were cut from blocks and mounted onto SuperFrost+ slides. Multiplex immunohistochemistry (m-IHC) staining using OPAL fluorophores was then performed according to the manufacturer's instructions (Akoya Bioscience, Marlborough, MA, USA). Briefly, the reagents were loaded into the Bond Rx Autostainer (Leica Biosystems, Wetzlar, Germany) for an entire cycle of approximately 12 hours. Tissue sections were baked, dewaxed and incubated in a 3% hydrogen peroxide (H_2O_2) solution (Merck EMSURE, Germany) to block endogenous peroxidases in the tissues. Subsequently slides were incubated with 1% bovine serum albumin (BSA) in Tris-Buffered Saline to block non-specific background binding. Slides were incubated iteratively with the primary antibodies including CD8 (1:4000 pH9), CD3e (1:600 pH6), CD103 (1:2000 pH9), for 30 min, the secondary antibody (OPAL polymer HRP Mouse + Rabbit) for 10 min, and the Tyramide conjugated OPAL fluorophores (570, 690 (1:150) and 780 (1:25) for 10 min. Finally, slides were incubated with spectral DAPI for 10 min. All antigen retrieval were performed at 97°C for 20 min whilst all other steps were performed at ambient temperature. Following the completion of staining, the slides were briefly rinsed in milliQ water and then manually cover slipped using Prolong Glass Antifade Mountant (Invitrogen, Carlsbad, USA).

The stained 4-plex OPAL m-IHC slides were imaged on the Phenoimager HT imaging system (AKOYA Biosciences, USA). The whole tissue section was spectrally imaged with on 20x objective. The optimal exposure settings were manually set for each tissue. Whole slide images were then unmixed to subtract auto-fluorescent signal and images exported as component tiffs using InForm software (v2.6.0, AKOYA biosciences, USA). Briefly, the

spectral library was created using multispectral images obtained from single stained slides for each marker and the associated fluorophore (DAPI, OPAL 570, 690 and 780) on InForm software (v2.6.0, AKOYA biosciences, USA) for downstream image analysis workflow. For Masson's trichrome staining 4-µm-thick sections were cut from FFPE blocks and incubated in Bouin's fixative for 60 minutes at 60°C, washed in water and stained with haematoxylin. Slides were washed and stained with 1% Ponceau 2 R and 1% Acid fucshin for 2 minutes. Slides were washed with water stained with 2% light green in 1% acetic acid for 5 minutes, washed with water, dehydrated and cover slips mounted.

Human histology and OPAL analysis

Human breast tissue preparation

Immune cells were interrogated to visualise the expression of CD3, CD8, CD69, CD103, and pan-cytokeratin (AE1/AE3) in cancer unaffected normal breast tissue, using the OPAL™ serial immunostaining protocol. Briefly, formalin-fixed paraffin embedded (FFPE) tissue sections were cut at 4um thickness and melted at 60°C for 45 minutes, followed by dewaxing in 3 changes of histolene for 11 minutes and 3 changes of 100% ethanol for 1 minute each and 70% alcohol for 1 minute. Leica Bond auto-stainer protocol was followed as per manufacturer instructions.

Antigen retrieval process

Heat-induced antigen retrieval was achieved using a microwave. Tissue sections were placed in a plastic hellendahl jar (Trajan Scientific Australia) in EDTA (pH 8) antigen retrieval buffer and citrate buffer (pH 6) antigen retrieval buffer for CD3 staining and brought to the boil at a 100% power for 50 seconds and at 10% power for 15 minutes. Tissue sections were then left to cool for 30 mins and washed in 0.02% TBST 3 times at 7 minutes each with gentle agitation.

Primary antibody staining

Sections were blocked in blocking buffer (Dako, X0909) for 10 minutes at room temperature prior to incubation with primary antibodies, or isotype controls. Sections were incubated for 30 mins at room temperature with mouse anti-human pan-cytokeratin (AE1/AE3); 1:1000 at Opal 480 (Isotype: mouse IgG1), rabbit anti-human CD3e (SP7); 1:500 at Opal 690 (Isotype: rabbit IgG), mouse anti-human CD8(4B11); Leica; 1:800 at 570 – 1:500 at Opal 570 (Isotype: mouse IgG2b),rabbit anti-human CD69 (EPR21814); Abcam at Opal 520 (Isotype: rabbit IgG), rabbit anti-human CD103 (EPR416602);Abcam; 1:1000 at Opal 780 (Isotype: rabbit IgG and cell-permeable DNA-binding dye (DAPI) obtained from Abcam. Following primary incubation; sections were washed in 0.02% TBST 5 times for 5 minutes each. Tissue sections were then incubated in 0.3% H_2O_2 for 10 mins following the first primary antibody incubation and washed in 0.02% TBST 3 times for 5 minutes each. Respective isotype antibody control expression was examined under similar conditions and were tested on matched human normal breast and in human tonsil lymphatic tissues.

Secondary antibody detection

All sections were incubated with secondary-HRP conjugated antibodies (Leica Bond autostianer protocol) at a dilution of 1:1000 for 10 mins at room temperature. Sections were washed 3 times for 5 minutes each in 0.02% TBST followed by signal amplification using 100ul of TSA Plus working solution per slide at a dilution of 1:50 in 1x amplification diluent, incubated at room temperature for 10 mins as specified by the manufacturer (Opal 6-Plex Manual Detection Kit - for Whole Slide Imaging, AKOYA, USA). Nuclei were counterstained with DAPI as per manufacturer instructions diluted from 10x spectral DAPI (AKOYA, USA) for 2 mins at room temperature. Sections were then washed twice in 0.02% TBST for 2 minutes each and mounted in Vecta shield hard set medium (Vector, USA) and left to dry flat for 20 mins in the absence of light.

Microscopy image analysis

OPAL multiplex immunohistochemistry (m-IHC) slides were imaged on the Pheno Imager HT (Polaris) (AKOYA Biosciences, USA). The acquired images were spectrally unmixed using inform v2 (AKOYA Biosciences, USA) into individual component tiff files. Whole slide images were then stitched in the HALO Image Analysis Platform version 3.6.4134 (Indica Labs, Inc., NM; USA). For human tissue, quantification of immune cells, specifically the $CD8^+$ T cell sub-populations in the mammary epithelial dense regions after excluding adipose dense regions across the entire tissue was performed using the HighPlex FL v4.2.3 module. For murine tissue, quantification of immune cell subsets was performed using the HighPlex FL v4.2.3 module after excluding lymph node regions within the surrounding tissues of interest. For distance between $ECAD^+$ epithelial cells and $CD8^+CD103^+$ T cells nearest neighbour was calculated on HALO Image Analysis Platform version 3.6.4134. Masson's trichrome positive staining was quantitated using QuPath 0.6[54].

RNA extraction and RT-qPCR analysis

Mammary fat pad tissue from C57BL/6 mice was manually minced and then homogenised in 500 µL TRIzol using metal bead lysing matrix (MP Biomedicals) on a FastPrep-24™ bead beating grinder and lysis system (MP Biomedicals). RNA was extracted from the homogenised tissue using the PureLink RNA Mini Kit (Invitrogen) as per the manufacturer's instructions. Total RNA was then quantified using a NanoDrop 2000 Spectrophotometer (Thermo Fisher Scientific). First-strand complementary DNA (cDNA) was synthesised from extracted RNA using the SuperScript IV VILO Master Mix with ezDNase enzyme (Invitrogen) following the manufacturer's instructions. This was performed on a T100 Thermal Cycler (Bio-Rad).

RT-qPCR was performed on the synthesised cDNA to assess relative gene expression using the TaqMan Gene Expression Assay with primers targeting *Gapdh*: Mm99999915_g1, *Tgfβ2*: Mm00436955_m, *Tnf*: Mm00443258_m1 and *Cxcl16*: Mm00469712_m1. All RT-qPCR reactions were performed on the StepOnePlus Real-Time PCR System (Thermo Fisher Scientific). *Gapdh* was used as the housekeeping gene. The $2^{-\Delta\Delta}$ Ct method was used for calculating relative gene expression[55].

Human, murine reagents and antibodies

Flow cytometry antibodies used for normal breast immunophenotyping include CD45-BV510, CD3-APCH7, CD103-BV421, CD8-BV605, PD-1-BV785, CCR7-BV711, CD3-BV711, CD4-BV650, CD69-PerCP-Cy5-5, Zombie red-PE-Tex-Red (Biolegend, San Diego, CA); HLA-ABC-PECy5, CD45-FITC, CD8-PE, CD45RA-FITC, (BD Biosciences, San Diego, CA).

Flow cytometry antibodies utilised for murine healthy MFP analysis and BC tumour immunophenotyping include CD45-APCCY7, TCRβ-BB700, TCRβ-BV786, CD8-BV711, CD8-BUV395, CD4-BUV805, CD44-BV605, CD62L-PECY7, CD62L-BUV737, CD69-BUV395, CD69-PE, CD103-FITC, CD103-PE, CD11B-BV711, CD11C-BV786, F4/80-EF450, MHC-II APC and Fixable dyes Fix-Yellow-BV510, Zombie NIR or Zombie red PE-Tex-Red (Biolegend, San Diego, CA).

Antibodies used for spectral flow cytometry immunophenotyping: CD45-PerCP, CD19-AF488, TCR$\gamma\delta$-PE-Cy7, NK1.1-BV570, CD3-Spark NIR685, TCRβ-BB700, CD8α -BUV395, CD4-BUV805, CD44-APCR700, CD62L-BUV737, CD69-PE, CD103-BV421, CD11b-BV711, CD11c-BV785, F480-APC, Ly6G-BV650, Ly6C-BV605, MHC-II-Spark Blue 550, Siglec F-PerCP-Fire 806, XCR1-Spark UV387,CD64-PE-Fire 744, and H-2K^{b}-OVA-tetramer-PE or H-2K^{b}-OVA-tetramer-APC were used to detect and track CD8^{+} T cells specific to SIINFEKL (OVA$^{257\text{-}264}$) peptide from ovalbumin (OVA) expressing tumour cells. Antibodies used to generate the CD8α^{+} T cell UMAP CD49a-BUV395, NK1.1-BUV563, CD8α -RB545, CD8b-BUV661, CD4-BUV805, Slamf6-BV421, CD103-BV480, CD44-BV510, Ly6C-BV570, KLRG1-BV605, CXCR3-BV650, CD39-BV711, PD1-BV750, CD244-BV785, TCR$\gamma\delta$-BB700, CD1D-tetramer-PE, CXCR6-PeDazzle594, CD69-PE-Cy7, CD45.2-SparkNIR685, CD62L-APCR700, TCRβ-APC-Cy7, CD38-APC-Fire810, Granzyme A-e450, TCF1-AF488, Granzyme B-APC, Tbet-PE/Fire810. Antibodies used to generate the AT3-OVA CD45^{+} UMAP were CD45-PerCP, CD19-AF488, TCR$\gamma\delta$-PE-Cy7, NK1.1-BV570, CD3-Spark NIR685, TCRβ-BB700, CD8α-BUV395, CD8β-BUV615, CD4-BUV805, CD44-APCR700, CD62L-BUV737, CD69-PE, CD103-BV421, CD11b-BV711, CD11c-BV785, F480-BUV661, Ly6G-BV650,

Ly6C-BV605, MHC-II-Spark Blue 550, Siglec F-PerCP-Fire 806, XCR1-Spark UV387,CD64-PE-Fire 744, and H-2K^{b}-OVA-tetramer-APC, CD39-PE-Dazzle594, PD1-RY586, PD-L1 RB780, LAG3-RB744, KLRG1-BV510, CD38-APCFire810, FOXP3-e450, Tbet-PE/Fire810, TCF1-RB705, CTLA-4-PE-Fire-640. A representative flow cytometry gating strategy of immune cells in murine tissue is shown in **Extended Data Figure 10b**.

Human MyBrCa clinical dataset

The full cohort described in Pan *et al* 2024 was filtered to cases with available RNAseq data, complete parity information and stage 1 – 3 diseases. Where patients had multiple synchronous tumours that underwent RNAseq, one sample per patient was selected giving preference to more complete clinical metadata and basal-like subtyping. Parity was defined as at least one live birth, and pregnancy-associated cancers were not excluded. The ESTIMATE immune infiltration scores calculated in the MyBrCa publication were used unmodified. An exploratory analysis of the associations of sequencing technical factors and known clinicopathological predictors influencing immune infiltration was conducted. An effect of sequencing batch on the ESTIMATE score was observed. There was otherwise variable impact of age at diagnosis, grade and stage on the ESTIMATE score that was not consistent across subtypes. Linear models were fit for each PAM50 subtype with the ESTIMATE score as the response (non-standardised) and parity (Yes or No), age at diagnosis (continuous), grade (grade 1/2 or grade 3) and stage (I, II or III) as covariates, using the 'lm' function in R. Following this, stepwise model selection using the Akaike Information Criterion (AIC) was performed using 'step' function. 3 cases without PAM50, 20 cases contained "normal-like" classification were excluded from the analysis. Selected covariates differed across subtypes, with parity being the only selected covariate for the basal-like subtype. The most parsimonious model was therefore considered to include parity (Yes or No) and sequencing batch (1 or 2) as covariates, and this was used for the final analysis for all subtypes. 95% confidence intervals for the estimated co-efficient were calculated with the 'confint' function in R (v1.11.0).

Use of the AIC selected models with more covariates specific to each subtype did not alter the conclusion about the influence of parity on immune infiltration in basal-like cases.

For the breastfeeding analysis, cases were divided into those with any history of breastfeeding regardless of duration (BF), no history of breastfeeding (no-BF), and nulliparous cases (N). 3-way ANOVA models were fit for each subtype with the ESTIMATE score as the response (non-standardised), breastfeeding status as the grouping variable (BF, no-BF or N) and sequencing batch (1 or 2) as a covariate as above using the 'aov' function in R (v1.11.0). Homogeneity of variances between groups in each subtype was confirmed with Bartlett's test using the 'bartlett.test' function in R. Departure from normality was tested with the Shapiro-Wilk test and examination of QQ plots. This showed minor departure from normality for the basal-like group ESTIMATE scores, not considered detrimental as there are at least 30 cases in each group. Between group mean differences were tested with Tukey's Honest Significant Difference method using the 'TukeyHSD' function in R, also reporting a 95% confidence interval for the mean difference and p-value adjusted for multiple comparisons with the Tukey-Kramer method.

For GSEA in the MyBrCa dataset, RNAseq was conducted and processed to raw counts as described in Pan *et al 2024*. The RNAseq counts were normalised using RUVIII[56] to remove batch effects and other unwanted variations. We then performed differential expression analysis comparing Parous and Nulliparous Basal samples as well as Breastfeeding Parous and Non-Breastfeeding Parous with the R package limma[47]. GSEA was performed using the fgsea (v1.30.0) library in R to detect gene set enrichment of the T_{RM} gene signatures, outputting a normalised enrichment score (NES) and false discovery rate (FDR).

The p values reported for subtype specific analyses were not corrected for multiple testing. The rationale for this is that these subtypes display clearly distinct characteristics, and there is a large body of literature supporting the differential biology of these subtypes and the

variable significance of immune infiltration between them. There is no reasonable expectation of equipoise regarding the influence of parity on immune infiltration across subtypes.

Human MyBrCa Immunohistochemistry

Immunohistochemical (IHC) stained FFPE tissue sections were prepared as per a standard diagnostic workflow. Four slides per tumour sample were stained with primary antibodies targeting specific antigens: anti-CD3 (clone 2GV6, predilute; Ventana Medical Systems), anti-CD8 (clone SP57, predilute; Ventana Medical Systems), with an additional slide stained with hematoxylin and eosin (H&E). The antibody staining was conducted using a Ventana Bench Mark XT Autostainer, and stained slides were digitised using an Aperio AT2 whole slide scanner.

Semi-automated scoring of immune markers

For $CD3^+$ and $CD8^+$ T cell IHC scoring, Aperio Imagescope (Leica Biosystems) was used to view the scanned images and 50 annotation boxes, each of size 0.7 mm x 0.4 mm, were drawn within the borders of the invasive tumour region. The borders of the invasive tumour region were determined with reference to the H&E-stained slides. Then, the Pixel Positive v9 algorithm implemented in Aperio Imagescope was used to calculate the number of positively stained pixels within the annotation boxes at a 0.16 colour saturation threshold. The number of positive pixels was then divided by the total number of pixels within the annotation boxes to obtain the proportion of the annotated area that was positively stained for $CD3^+$ and $CD8^+$ immune cell types.

Human MyBrCa data analysis

beta regression was used to model the relationship between T cell density (represented as a proportion of stained to total pixels) and parity/breastfeeding, as implemented in the R package betareg (v3.2-1). Exploratory analysis determined that age at diagnosis of cancer and tumour grade were associated with T cell density, and these were used as covariates in

addition to parity/breastfeeding as predictor variable. The emmeans R package (v1.11.0) was used to calculate the average marginal effect and confidence intervals between groups.

Breastfeeding patient cohort

Patient data was acquired from kConFab[57]. Women diagnosed with breast cancer over the age of 18, with a known germline pathogenic variant who were diagnosed between the years of 1980 and 2022. Only patients who had hormone receptor negative primary breast cancers, had at least 1 full term pregnancy and confirmed breastfeeding status (yes/no) were included for survival analysis. Patients who had subsequent pregnancies after breast cancer diagnosis were not included in the cohort. All relevant clinical data is shown in **SI. Table 4** Data was not blinded. Breastfeeding duration was recorded based on total length across one or more children, where available.

Stromal tumour infiltrating lymphocyte scoring

TILs were scored in accordance with the guidelines from TILs International Working Group as percentage infiltration of the tumoural stroma Salgado *et al* 2015. from digitised H&E slides. Slides were acquired for where possible (n=136/270)

To account for potential confounding effects of patient age on stromal TIL percentages, we performed an age-adjusted analysis. Stromal TIL data were obtained from the updated dataset containing clinical annotations and pathological assessments of breast cancer patients. The remaining patients were stratified into defined breastfeeding duration groups (0, <6 months, 6–12 months and >12 months).

We adjusted the stromal TIL percentages for patient age using a linear regression model, fitting stromal TIL percentage as the dependent variable and age at diagnosis as the independent predictor. Adjusted stromal TIL values were derived from the residuals of this linear model, standardised to the mean intercept value, effectively removing linear age-related

variation. A Kruskal–Wallis test was used to evaluate differences in age-adjusted stromal TIL percentages across breastfeeding groups.

Breastfeeding Patient Survival Analysis

The analysis examined the association between breastfeeding and survival outcomes utilising both univariate and multivariate Cox proportional hazards models. Survival data was censored at 15 years, resulting in 45 observed events. Univariate analyses evaluated the direct effect of breastfeeding status on overall survival, while multivariate analyses controlled for potential confounders including patient age at breast cancer diagnosis, years from breast cancer diagnosis from last live birth (≤10yrs vs >10yrs), chemotherapy treatment (Y/N), and mastectomy (Y/N). Robust variance estimates were applied, and the proportional hazards assumption was tested using the Schoenfeld residuals test.

PB-T_{RM} signature and TILs correlation

We accessed the ht-seq gene counts from TCGA using the Broad Institute Firehose platform. The counts were normalised to remove library size effects using edgeR[58]. The PB-T_{RM} signature scores were computed using the genefu package[46] in R. Stromal TILs were scored for each TCGA case by a pathologist (R.S.) using whole slide H&E images according to established methods, Salgado *et al* 2015. PB-T_{RM} signature scores and TILs were correlated using the Spearman's correlation coefficient in R.

PB-T_{RM} signature score and survival

We accessed the normalised microarrays from the METABRIC study Curtis *et al* 2012 using cBioportal[59] and computed the PB-T_{RM} signature scores with genefu (2.36.0)[46]. Samples were stratified into two groups around the median signature score (high vs low) and Kaplan-Meier survival estimates were compared between groups using the log-rank test. Hazard Ratios were also calculated in R using the PB-T_{RM} signature scores by fitting a Cox Proportional-Hazards regression model.

Statistics, Codes and Reproducibility

All statistical analyses and the associated information relating error bars, box plots and sample size used to determine statistical significance were provided in the figure legends and statistical tools utilised were given in respective methods section. **Main Fig. 1b,** Proportions of $CD45^+$, $CD3^+$, $CD8^+$ T cells over total cells were provided, and $CD69^+CD103^-$ and $CD69^+CD103^+$ T cells over total $CD45RA^-CCR7^-CD8^+$ T cells (Y-axes) by flow cytometry from normal breast of women with high BC risk. Horizontal bar shows median, hinges represent IQR and whiskers extend to the most extreme dot point within 1.5xIQR, and points beyond show outliers. OPAL microscopy data associated to representative **Main Fig. 1c,** were also verified by flow cytometry and OPAL verification cohort were repeated n=5 per group in independent (N vs P) human breast tissue samples with comparable results, single colour stained images with markers and the collated data provided in **Extended Data Fig. 2a,b**. All experiments were reproduced twice, and the results represent two combined biologically independent experiments unless specified. Breastfeeding patient cohort statistical information, statistical analyses of human data were conducted using R v4 and for murine data, we used Graphpad Prism v9. Violin plots, with error bars representing the IQR, were used to compare immune cell proportions. No codes or software tools were specifically developed for this study. Plots were produced with the ggplot2 R package (v3.5.1), and data input and processing were performed with dplyr 1.1.2, tidyr 1.3.0, readxl 1.4.3, readr 2.1.4 and magrittr 2.0.3.

Data Access

Processed and raw bulk RNA Sequencing counts resulting from FACS sorted $CD69^+CD103^+CD8^+$T cells used to generate the PB-T_{RM} signature can be accessed through GEO: GSE271307. Single-cell RNA sequencing data and all associated cell annotations were available from the original publication Reed *et al 2024*[15]. Code associated with analyses can be accessed at https://doi.org/10.5281/zenodo.17120517. Data associated with human

normal breast and murine experimental analyses are available online under supplementary Source data. Clinical metadata and sequencing data for the human MyBrCa dataset are accessible with permission as per the original publication Pan *et al 2024*[28]. Human breastfeeding data with associated overall survival and TIL scores are provided by kConFab. As this is an ongoing prospective cohort, the ethics pertaining to this data requires that data access be approved via the process described at https://www.kconfab.org/Data%20Access/AppProcess.html. using the contact details provided at https://www.kconfab.org/contact_us.html. The corresponding author (S Loi) can assist requesting parties in facilitating applications to access the data. Responses are provided within a 2-month time frame. The authors declare that all other data supporting this study are provided in the Supplementary Materials.

Methods References

46. Gendoo, D.M.A., *et al.* Genefu: an R/Bioconductor package for computation of gene expression-based signatures in breast cancer. *Bioinformatics* **32**, 1097-1099 (2015).
47. Ritchie, M.E., *et al.* limma powers differential expression analyses for RNA-sequencing and microarray studies. *Nucleic Acids Res* **43**, e47 (2015).
48. Korotkevich, G., *et al.* Fast gene set enrichment analysis. *bioRxiv*, 060012 (2021).
49. Hao, Y., *et al.* Dictionary learning for integrative, multimodal and scalable single-cell analysis. *Nature Biotechnology* **42**, 293-304 (2024).
50. Alquicira-Hernandez, J. & Powell, J.E. Nebulosa recovers single-cell gene expression signals by kernel density estimation. *Bioinformatics* **37**, 2485-2487 (2021).
51. Aibar, S., *et al.* SCENIC: single-cell regulatory network inference and clustering. *Nature Methods* **14**, 1083-1086 (2017).
52. Bouchard, G., *et al.* Stimulation of triple negative breast cancer cell migration and metastases formation is prevented by chloroquine in a pre-irradiated mouse model. *BMC Cancer* **16**, 361 (2016).
53. Beavis, P.A., *et al.* Dual PD-1 and CTLA-4 Checkpoint Blockade Promotes Antitumor Immune Responses through CD4(+)Foxp3(-) Cell-Mediated Modulation of CD103(+) Dendritic Cells. *Cancer Immunol Res* **6**, 1069-1081 (2018).
54. Bankhead, P., *et al.* QuPath: Open source software for digital pathology image analysis. *Sci Rep* **7**, 16878 (2017).
55. Livak, K.J. & Schmittgen, T.D. Analysis of relative gene expression data using real-time quantitative PCR and the 2(-Delta Delta C(T)) Method. *Methods* **25**, 402-408 (2001).

56. Molania, R.*, et al.* Removing unwanted variation from large-scale RNA sequencing data with PRPS. *Nat Biotechnol* **41**, 82-95 (2023).
57. Thorne, H., Mitchell, G. & Fox, S. kConFab: a familial breast cancer consortium facilitating research and translational oncology. *J Natl Cancer Inst Monogr* **2011**, 79-81 (2011).
58. Robinson, M.D., McCarthy, D.J. & Smyth, G.K. edgeR: a Bioconductor package for differential expression analysis of digital gene expression data. *Bioinformatics* **26**, 139-140 (2009).
59. Gao, J.*, et al.* Integrative analysis of complex cancer genomics and clinical profiles using the cBioPortal. *Science signaling* **6**, pl1-pl1 (2013).

Extended Data Figure 1. Immune cell types by parity status in cancer unaffected human breast tissue

a-e. Abundance of immune cell types quantified from scRNAseq by parity status in human normal breast tissue shown as ratio of cell type in women of average breast cancer risk. Cell types are annotated as per Reed *et al*[15]. Y-axes indicate cell type frequency as calculated by cell sub-populations as indicated over total epithelial cells. **a,** Macrophages, n=170 women (N, n=53) vs (P, n=117), M1 and M2 macrophage cell sub-populations, n=105 women (N, n=30) vs (P, n=75). **b,** Monocytes, n=105 women (N, n=30) vs (P, n=75). **c,** Dendritic cells n=124 women (N, n=37) vs (P, n=87). **d,** B cells n=123 women (N, n=37) vs (P, n=86). **e,** Fibroblasts, n=170 women (N, n=53) vs (P, n=117), Fibroblast matrix associated cells, n=102 women, (N, n=27) vs (P, n=75) and Fibroblast $SFRP4^+$ sub-populations, n=90 women (N, n=25) vs (P, n=65). Violin plots show data distribution with boxplots indicate IQR extension from Q1 to Q3 and median as a white bar, whiskers show minimum and maximum within 1.5 times the IQR and datapoints show outliers. Two-sided Wilcoxon rank sum test, unadjusted exact p-values are shown.

Extended Data Figure 2. OPAL image of T cells in cancer unaffected human breast

a. Representative OPAL multiplex immunofluorescence single-colour and merged images of cancer unaffected normal breast tissue from nulliparous and parous women stained for DAPI, pan-cytokeratin (AE1/AE3) CD3, CD8, CD69, and CD103. scale bar is defined on the panels. **b.** Quantification of OPAL immunofluorescence in cancer unaffected human normal breast (n=5 per group) for T cells sub-populations in mammary regions indicating density of $CD3^+$, $CD8^+$ and $CD69^+CD103^+CD8^+CD3^+$ T cells per mm^2 from nulliparous (N) and parous(P) women. Data in graphs represent mean ±SEM, two-sided Wilcoxon rank-sum test and dots points represent indicated immune cell quantities from independent normal breast tissue samples. **c.** Immune cell abundance (right) and enrichment of PB-T_{RM} gene signature (left) in the T_{EM} and T_{RM}-like cell clusters as annotated by originating publication Reed *et al*[15]. Effector

CD8⁺ T cells (n=26,333 cells) from nulliparous vs parous women. Wilcoxon rank-sum test (two-sided) and unadjusted exact p-value is shown.

Extended Data Figure 3. Immune cell subsets in healthy murine mammary tissue.

a. Frequency of indicated immune cell subsets among all CD45⁺ cells from the MFP of virgin (n=9) and d28-inv (n=12) C57BL/6 mice. **b.** Number of indicated immune cell subsets per gram of MFP from virgin (n=9) and d28-inv (n=12) C57BL/6 mice. **c.** Number of indicated immune cell subpopulations per gram of MFP from virgin (n=8) and d10-FW (n=8) BALB/c mice. Data in graphs represent mean ±SEM, results represent two combined independent experiments. Statistical significance determined by two-sided Mann-Whitney test and exact p values are shown.

Extended Data Figure 4. CD8⁺ T cell sub-populations in healthy murine MFP.

a.Top: UMAP of merged CD8α⁺ T cells generated by flow cytometry data from the MFP of virgin (n=8) and d28-inv (n=9) C57BL/6 mice with three enriched clusters (C1, C2, C3) as indicated. Each dot represents an individual cell. Feature plots showing expression of indicated markers projected on UMAP of CD8α⁺ T cells are presented in the bottom layout.

Extended Data Figure 5. CD8⁺T_{RM}-like cells in healthy murine MFP

a.Relative expression of indicated expressed gene transcripts relative to *GAPDH* control isolated from MFP from virgin (n=10) vs d28-inv (n=9) timepoints from C57BL/6 mice. **b.** Representative OPAL images indicating the presence of DAPI⁺, CD3⁺, CD8⁺, CD103⁺ cells (white dots) in the MFP of virgin, d10-FW and D28-inv C57BL/6 mice. Blue regions indicate local lymph node and yellow represent mammary fat pad tissue boundary. **c.** Total number of CD3⁺CD8⁺CD103⁺ T cells in the 4th MFP of virgin (n=7), d10-FW (n=4) and d28-inv (n=6) C57BL/6 mice measured by OPAL microscopy per mammary fat pad section. **d.**

Representative OPAL images indicate the single-colour staining of DAPI, E-cadherin (ECAD), CD3, CD8 and CD103 on T cells in the MFP of virgin, d10-FW and D28-inv C57BL/6 mice. **e.** Mean distance between $ECAD^+$ cells and the closest $CD3^+$ $CD8^+$ $CD103^+$ T cells of virgin (n=7), d10-FW (n=4) and d28-inv (n=6) C57BL/6 mice. Data in graphs represent mean ±SEM, results represent two combined independent experiments. Statistical significance determined by two sided Mann-Whitney test (a) or Kruskal-Wallis test (c, e). Exact p values are shown

Extended Data Figure 6. Immune cell infiltration in TNBC murine mammary tumours.

a.Numbers of indicated immune cell sub-populations per gram of AT3-OVA tumour from virgin (n=9) and d28-inv (n=10) C57BL/6 mice. **b.** Numbers of indicated immune cell subpopulations per gram of AT3-OVA tumour from virgin (n=8) and d10-FW (n=8) C57BL/6 mice. **c.** Numbers of indicated immune cell subpopulations per gram of D2A1 tumour from virgin (n=8) and d10-FW (n=8) BALB/c mice. **d.** Numbers of indicated immune cell subpopulations per gram of D2A1 tumour from virgin (n=6) and d28-inv (n=7) BALB/c mice. Data in graphs represent mean ±SEM, results represent two combined independent experiments. Statistical significance determined by two-sided Mann-Whitney test. Exact p values are shown.

Extended Data Figure 7. TNBC tumour growth and immune infiltration in murine models.

a.Tumour growth (left) and endpoint tumour volume (right) of AT3-OVA cells in the 4^{th} MFP of $RAG2^{-/-}\gamma c^{-/-}$ mice pre-inoculated with naive OT-I cells seven days prior to mating in d10-FW (n=4) and age-matched virgin (n=4) control mice. **b.** Numbers of indicated immune cell populations in $RAG2^{-/-}\gamma c^{-/-}$ mice pre-inoculated with effector OT-I cells seven days prior to mating in d28-inv (n=10) and age-matched virgin (n=10) control mice. **c.** Numbers of indicated immune cell subpopulations per gram of AT3-OVA tumour from virgin (n=6) and d10-FW (n=6) $RAG2^{-/-}\gamma c^{-/-}$ mice at four weeks post tumour cell injection. **d.** Tumour growth (left) and endpoint

tumour burden (right) of AT3-OVA cells in the 4th MFP of $RAG^{-/-}1^{-/-}$ mice. Mice were injected with $20x10^6$ effector gBT-I cells or PBS control eight weeks prior to injection of AT3-OVA cells (n=5 per group for tumour growth and 10 for endpoint weight). Data in graphs represent mean ±SEM. Results are representative of n=2 independent experiments (a, d left) or two combined independent experiments (b-d right). Statistical significance determined by two-sided Mann-Whitney test. Exact p values are shown.

Extended Data Figure 8. T cell depletions and TIL differences in TNBC murine models

a.Number of indicated immune cells per gram of AT3-OVA tumour from virgin mice treated with isotype control(n=16), anti-CD4 (n=12), anti-CD8α (n=9), anti-CD8β(n=12) or anti-CD4/CD8a (n=14). **b.**Number of indicated immune cells per gram of AT3-OVA tumour from d28-inv mice treated with isotype control(n=16), anti-CD4(n=13), anti-CD8α(n=9), anti-CD8β (n=14) or combined anti-CD4/CD8α(n=14). **c.**AT3-OVA endpoint tumour weight in C57BL/6 mice in virgin (n=16) and d28-inv(n=16) isotype treated controls. **d.**Number of indicated immune cells per gram of AT3-OVA tumour from d28-inv virgin (n=16) and d28-inv (n=16) mice treated with isotype control. **e.**Representative UMAP of 20,000 $CD45^+$ immune cells by flow cytometry from AT3-OVA tumours of C57BL/6 d28-inv isotype control and CD4 depleted mice with two enriched clusters (C1,C2) indicated and $CD4^+$ T cells highlighted. Each dot represents an individual cell. **f.**UMAP plots of indicated $CD45^+$ cells from AT3-OVA tumours in d28-inv treated with isotype, anti-CD4, anti-CD8α, anti-CD8β or anti-CD4/CD8α. **g.**Frequency of cluster 1 among all $CD45^+$ cells in AT3-OVA tumours from d28-inv isotype (n=8) and CD4 depleted (n=7) C57BL/6 mice. **h.**Relative expression of indicated markers in cluster 1 relative to all $CD45^+$ cells from d28-inv isotype (n=8). **i.**Frequency of cluster 2 among all $CD45^+$ in AT3-OVA tumours from d28-inv isotype (n=8) and CD4 depleted(n=7) C57BL/6 mice. **j.**Relative expression of indicated markers in cluster 2 relative to all $CD45^+$ from d28-inv isotype control mice(n=8). **k.** Number of indicated immune cells per gram of AT3-OVA tumour from d28-inv mice treated with isotype (n=16) or anti-CD4(n=13). **l.**Representative images of

AT3-OVA tumours stained with Masaon's trichrome. Arrows indicate positive green staining of collagen in virgin (left) and d28-inv (right) tissue. **m.**Proportion of Masson's trichrome staining in AT3-OVA tumours from virgin(n=6) and d28-inv (n=5) C57BL/6 measured by Masson's trichrome staining. Two combined independent experiments (a-c,k-m) representative of two independent experiments (e-j). mean ±SEM, two-sided Mann-Whitney test. Exact p values are shown.

Extended Data Figure 9. Parity, breastfeeding and TIL associations in human breast cancer subtypes

a. Breastfeeding cohort multivariate analysis with clinical prognostic factors shown (n=270). OS events were censored at 15 years follow up and adjusted for breastfeeding status (BF), age at diagnosis (Age.dx), years since last live birth to BC diagnosis (time since last birth), and treatment with chemotherapy (treatment_chemo) or mastectomy (treatment_mastectomy). Hazard ratios are presented with 95% confidence intervals, shown as squares and horizontal lines, respectively. **b.** PB-T_{RM} signature correlation with tumour infiltrating lymphocyte (TIL) counts in TNBC (Basal subtype, n=136) from the TCGA dataset. *R* value indicate Spearman's correlation coefficient (two-sided p value from correlation test). **c.** Enrichment of the PB-T_{RM} signature in the indicated BC subtypes from the Metabric dataset, Basal (n=329), HER2 (n=240), LumA (n=718) and LumB (n=488). Kruskal Wallis test, p-value shown is unadjusted, **d.** Kaplan–Meier survival analysis indicates disease-free survival and **e.** overall survival from (n = 329) primary basal-like/TNBCs with prognostic separation according to PB-T_{RM} signature from parous normal breast tissue. Log-rank, p-values and hazard ratios are shown. **f.** Intratumoural T cell density in HER2 and Luminal BC subtypes determined by immunohistochemistry for $CD8^+$ and $CD3^+$ in MyBrCa dataset, comparing nulliparous (N) and parous (P) women with differing breastfeeding histories prior to cancer diagnosis (bf: any recorded breastfeeding activity). $CD8^+$ and $CD3^+$ T cell density quantified as ratio of stain-positive pixels to all pixels within tumour margins, represented as a percentage. Modelled with

beta regression adjusting for covariates of age at diagnosis and tumour grade. Unadjusted p values with the AME for each group compared to N are presented. Box plots: Horizontal bar shows median, hinges represent IQR, and whiskers extend to the most extreme dot point within 1.5xIQR, and points beyond show outliers. Individual points show data from each case, coloured according to the status shown on the x-axis. Exact p values are shown.

Extended Data Figure 10. **Representative flow cytometry gating strategies**

a. Immunophenotyping of cancer-unaffected human normal breast tissue (**Main Fig. 1b**) Immunophenotyping of healthy C57BL/6 murine immune cell phenotyping of mammary tissue are shown from cells gated based on morphology (FSC-A, SSC-A) and singlets (FSC-H, FSC-A). (**Main Fig. 2)**

Acknowledgements

The authors would like to acknowledge the Peter MacCallum Cancer Centre Flow Cytometry Facility, Amanda Lee, Stuart Bencraig and Tim Semple from Molecular Genomics Core, Centre Animal Research Platform, Centre for Advanced Histology and Microscopy at the Peter MacCallum Cancer Centre. Australian genome research facility (AGRF, Melbourne, Australia) for their assistance with RNA sequencing. We thank Richard Young and David Byrne for the OPAL microscopy reagents and histology sectioning support. We also thank Chris Mintoff, Michael Neeson, Tania Tan, Valerie Setiono for assistance with human breast tissue processing. We also thank Melrine Pereira for providing D2A1 cells. We sincerely thank Kconfab team members Genna Glavich, Alexandra Smith, Lody Mokdsi and Eveline Niedermayr for their ongoing support. We thank Jeannette Parrodi for her administrative support.

This work was supported by the Mark Foundation ASPIRE II Award (APP ID: 5820526561), Australia, Cancer Council Victoria and the Department of Health, Victoria, Australia. S.Loi is

supported by the National Breast Cancer Foundation of Australia (NBCF) (APP ID: EC-17-001), the Breast Cancer Research Foundation, New York (BCRF (APP ID: BCRF-21-102) and a National Health and Medical Council of Australia (NHMRC), Investigator Grant (APP ID: 1162318), and the Peter MacCallum Cancer Centre Foundation. P.S. is supported by a National Health and Medical Council of Australia (NHMRC) Investigator Grant (APP ID: 2017477) and the Peter MacCallum Cancer Centre Foundation. B.V. is supported by a Postdoctoral Research Fellowship from Cancer Council Victoria and the Department of Health, Victoria, Australia. P.K.D is supported by a National Health and Medical Research Council Principal Research Fellowship (APP ID: 1136680). L.K.M. is a Senior Medical Research Fellow supported by the Sylvia and Charles Viertel Charitable Foundation.

Author Contributions

B.V, F.C, P.S, M.A.H, performed primary human and murine experiments, analysed results, coordinated the project, and wrote the research manuscript. F.C, P.S, J.W and J.P generated programming scripts and analysed the bioinformatics results. E.B and D.C, performed murine experiments, dosing, tumour cell injections, associated procedures and maintenance of murine models. M.R.O, C.G, M.H, T.N.B and S.S supported with interpretation of results and performed experiments. J.K, J.B.D, L.G, K.C, S.T, H.Y, R.I, M.J, supported with experiments. kConFab Investigators contributed to the recruitment of participants and coordinated biospecimen acquisition, clinical data curation and governance. H.T. from KConFab contributed to recruitment of participants, biospecimen acquisition, clinical data curation. R.S, H.T, C.P, S.N, T.H, T.S., J.V, P.J.N, P.K.D and LKM provided scientific expertise. All authors approved the final research manuscript. S.L. as lead senior author conceived, led and coordinated the project, and provided the project funding.

Conflict of Interest

P.S has acted as a consultant (not compensated) to Roche-Genentech and received research funding to his institution from Roche-Genentech.

S.Loi receives research funding to her institution from Novartis, Bristol Meyers Squibb, Merck, Puma Biotechnology, Eli Lilly, Nektar Therapeutics, Astra Zeneca, Roche-Genentech and Seattle Genetics. S.Loi has acted as consultant to Seattle Genetics, Novartis, Bristol Meyers Squibb, Merck, AstraZeneca, Eli Lilly, Roche-Genentech, Aduro Biotech, GlaxoSmithKline, Silverback Therapeutics, G1 Therapeutics, PUMA Biotechnologies, Pfizer, Gilead Therapeutics, Daiichi Sankyo, Amuni and Tallac Therapeutics. PKD receives research funding from Myeloid Therapeutics, Prescient Therapeutics and Bristol-Myers Squibb.

Additional Information

Supplementary Information is available for this paper.

Correspondence and requests for materials should be addressed to Professor Sherene Loi – sherene.loi@petermac.org

List of the kConFab consortium authors' and affiliations

kConFab investigators and consortium members

David Amor^10, Lesley Andrews^11, Yoland Antill^1, Rosemary Balleine^12, Jonathan Beesley^13, Ian Bennett^14, Michael Bogwitz^15, Simon Bodek^16, Leon Botes^11, Meagan Brennan^17, Melissa Brown^18, Michael Buckley^19, Jo Burke^20, Phyllis Butow^21, Liz Caldon^22, Ian Campbell^1, Michelle Cao^23, Anannya Chakrabarti^24, Deepa Chauhan^25, Manisha Chauhan^26, Georgia Chenevix-Trench^13, Alice Christian^27, Paul Cohen^28, Alison Colley^29, Ashley Crook^30, James Cui^31, Eliza Courtney^30, Margaret Cummings^32, Sarah-Jane Dawson^1, Anna deFazio^12, Martin Delatycki^16, Rebecca Dickson^30, Joanne Dixon^27, Stacey Edwards^18, Gelareh Farshid^33, Andrew Fellows^1, Georgina Fenton^34, Michael Field^30, James Flanagan^35, Peter Fong^36, Laura Forrest^15, Stephen Fox^1, Juliet French^18, Michael Friedlander^11, Clara Gaff^15, Mike Gattas^37, Peter George^38, Sian Greening^39, Marion Harris^1, Stewart Hart^40, Philip Harraka^31, Nick Hayward^13, John Hopper^41, Cass Hoskins^15, Clare Hunt^40, Paul James^42, Mark Jenkins^41, Alexa Kidd^27, Judy Kirk^12, Jessica Koehler^11, James Kollias^33, Sunil Lakhani^37, Mitchell Lawrence^31, Jason Lee^13, Shuai Li^41, Geoff Lindeman^8, Jocelyn Lippey^43, Lara Lipton^44, Liz Lobb^25, Sherene Loi^1, Graham Mann^12, Deborah Marsh^45, Sue-Anne McLachlan^46, Bettina Meiser^11, Roger Milne^47, Sophie Nightingale^6, Shona O'Connell^40, Sarah O'Sullivan^28, David Gallego-Ortega^22, Nick Pachter^15, Jia-Min Pang^1, Gargi Pathak^28, Briony Patterson^23, Amy Pearn^48, Kelly Phillips^1, Ellen Pieper^15, Susan Ramus^45, Edwina Rickard^12, Abi Ragunathan^12, Bridget Robinson^49, Mona Saleh^11, Anita Skandarajah^1, Elizabeth Salisbury^11, Christobel Saunders^47, Jodi Saunus^18, Peter Savas^1, Rodney Scott^50, Clare Scott^8, Adrienne Sexton^15, Joanne Shaw^25, Andrew Shelling^36, Shweta Srinivasa^12, Peter Simpson^18, Melissa Southey^41, Amanda Spurdle^13, Jessica Taylor^15, Renea Taylor^31, Heather Thorne^1, Alison Trainer^11, Kathy Tucker^11, Jane Visvader^8, Logan Walker^13, Rachael Williams^11, Ingrid Winship^15, Mary-Ann Young^22, Milita Zaheed^11

Affiliations for kConFab Investigators (continue from 1–9 title page)

^10 Genetic Health Services Victoria, Royal Children's Hospital, Melbourne VIC 3050, Australia.
^11 Hereditary Cancer Clinic / Prince of Wales Hospital, Randwick NSW 2031, Australia.
^12 Westmead Hospital and Westmead Institute for Cancer Research, Westmead NSW 2145, Australia.
^13 QIMR Berghofer Medical Research Institute, Herston QLD 4006/4029, Australia.
^14 Silverton Place, 101 Wickham Terrace, Brisbane QLD 4000, Australia.
^15 Familial Cancer Centre and Genomic Medicine, The Royal Melbourne Hospital / VCCC, Parkville VIC 3050, Australia.
^16 Austin Health, Heidelberg/Melbourne VIC 3081, Australia.
^17 NSW Breast Cancer Institute, Westmead NSW 2145, Australia.
^18 The University of Queensland, St Lucia/Herston, QLD, Australia.
^19 Molecular and Cytogenetics Unit, Prince of Wales Hospital, Randwick NSW 2031, Australia.
^20 ICON Cancer Care, Hobart TAS 7000, Australia.
^21 Medical Psychology Unit, Royal Prince Alfred Hospital, Camperdown NSW 2050, Australia.
^22 Garvan Institute of Medical Research / The Kinghorn Cancer Centre, Darlinghurst NSW 2010, Australia.
^23 Tasmanian Clinical Genetics Service, Royal Hobart Hospital, Hobart TAS 7001, Australia.
^24 Specialist Breast Cancer Surgery, Richmond VIC 3121, Australia.

^25 School of Psychology, The University of Sydney, Camperdown NSW 2006, Australia.
^26 St Vincent's Hospital Cancer Genetics Clinic, The Kinghorn Cancer Centre, Sydney NSW, Australia.
^27 Central Regional Genetics Service, Wellington Hospital, Wellington, New Zealand.
^28 St John of God Subiaco Hospital / Genetic Services of Western Australia, Subiaco WA 6008, Australia.
^29 Department of Clinical Genetics, Liverpool Hospital, Liverpool NSW 2170, Australia.
^30 Department of Clinical Genetics, Royal North Shore Hospital, St Leonards NSW 2065, Australia.
^31 Monash University, Clayton VIC 3168/3800, Australia.
^32 Department of Pathology, University of Queensland Medical School, Herston QLD 4006, Australia.
^33 SA Pathology / Royal Adelaide Hospital, Adelaide SA 5000, Australia.
^34 South West Family Cancer Clinic, Liverpool Hospital, NSW, Australia.
^35 Imperial College London, London W12 0NN, UK.
^36 Auckland City Hospital / University of Auckland, Auckland, New Zealand.
^37 Queensland Clinical Genetic Service / Royal Brisbane and Women's Hospital, Herston QLD 4029, Australia.
^38 Canterbury Health Laboratories, Christchurch, New Zealand.
^39 Illawarra Cancer Centre, Wollongong Hospital, Wollongong NSW 2521, Australia.
^40 Southern Health Familial Cancer Centre, Monash Medical Centre, Clayton VIC 3168, Australia.
^41 Centre for Epidemiology and Biostatistics / Melbourne School of Population and Global Health, The University of Melbourne, Carlton VIC 3053, Australia.
^42 Genetic Health Services (Monash Medical Centre), Clayton VIC, Australia.
^43 Department of Surgery, St Vincent's Hospital, Melbourne VIC, Australia.
^44 Medical Oncology and Clinical Haematology Unit, Western Health, Footscray VIC, Australia.
^45 School of Women's and Children's Health / Lowy Cancer Research Centre, UNSW Sydney, Kensington NSW, Australia.
^46 Department of Oncology, St Vincent's Hospital, Fitzroy VIC 3065, Australia.
^47 The Royal Melbourne Hospital / University of Western Australia / Department of Surgery, Parkville VIC / Perth WA, Australia.
^48 The Gene Council, North Perth WA 6906, Australia.
^49 Christchurch Hospital, Christchurch, New Zealand.
^50 Hunter Area Pathology Service, John Hunter Hospital, Newcastle NSW 2310, Australia.

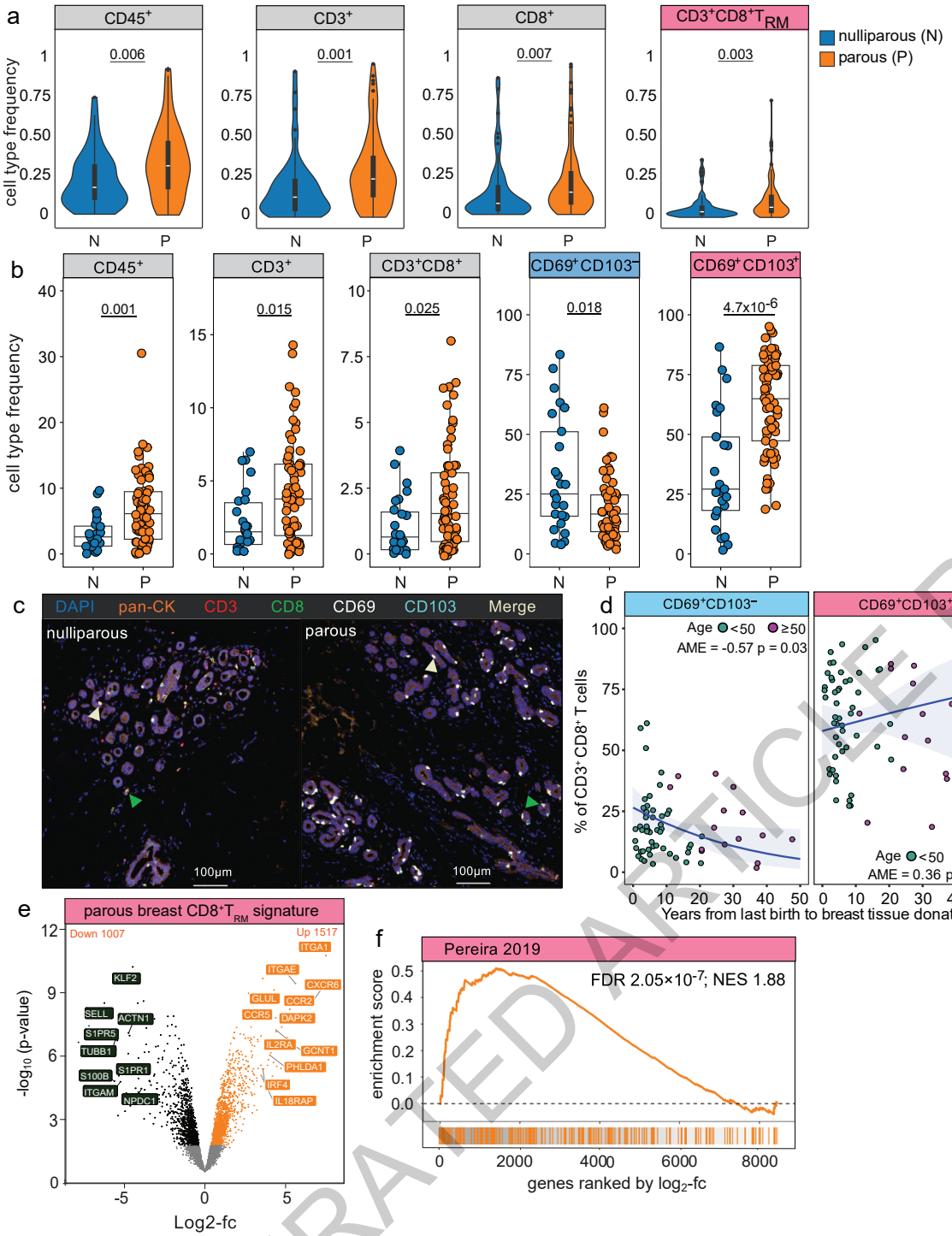

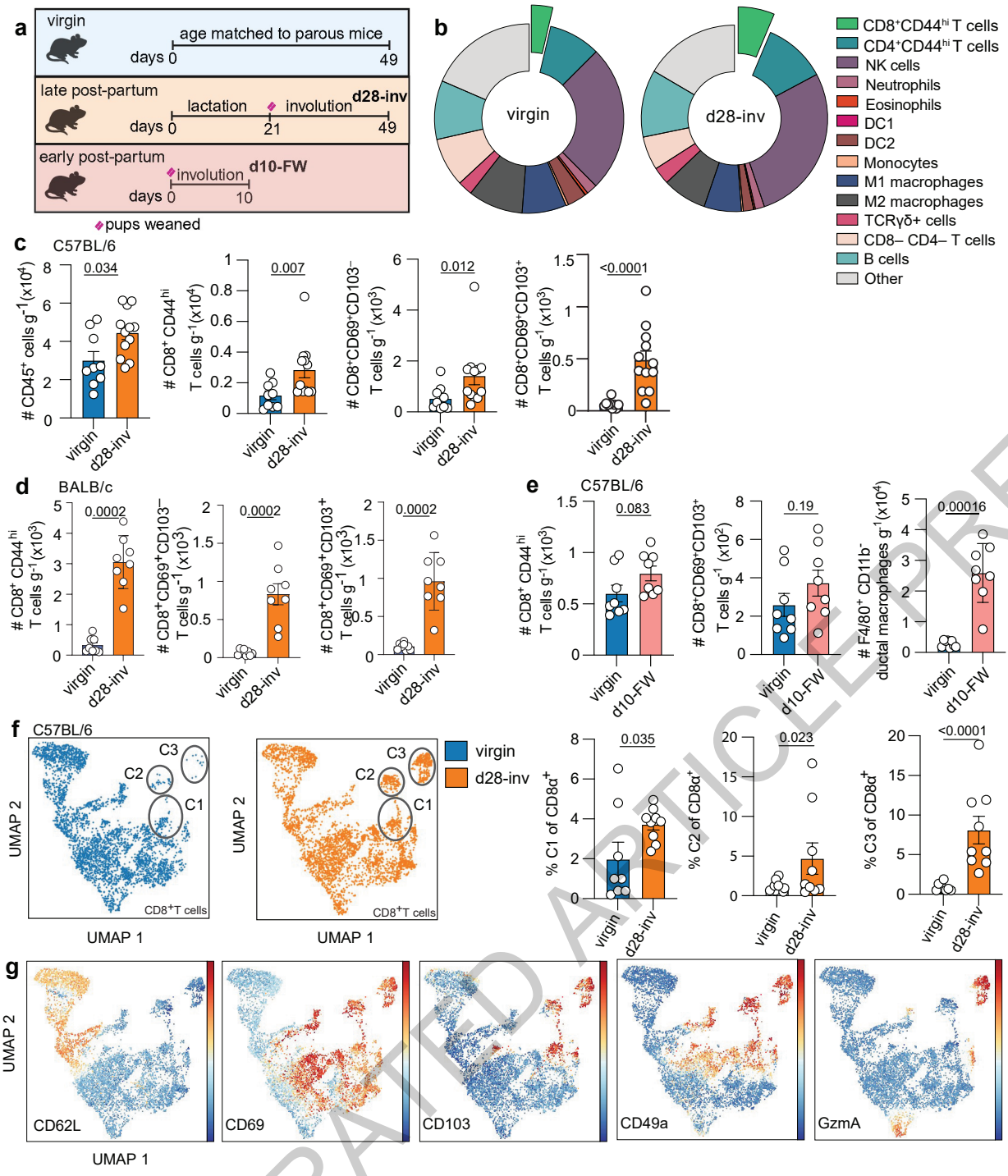

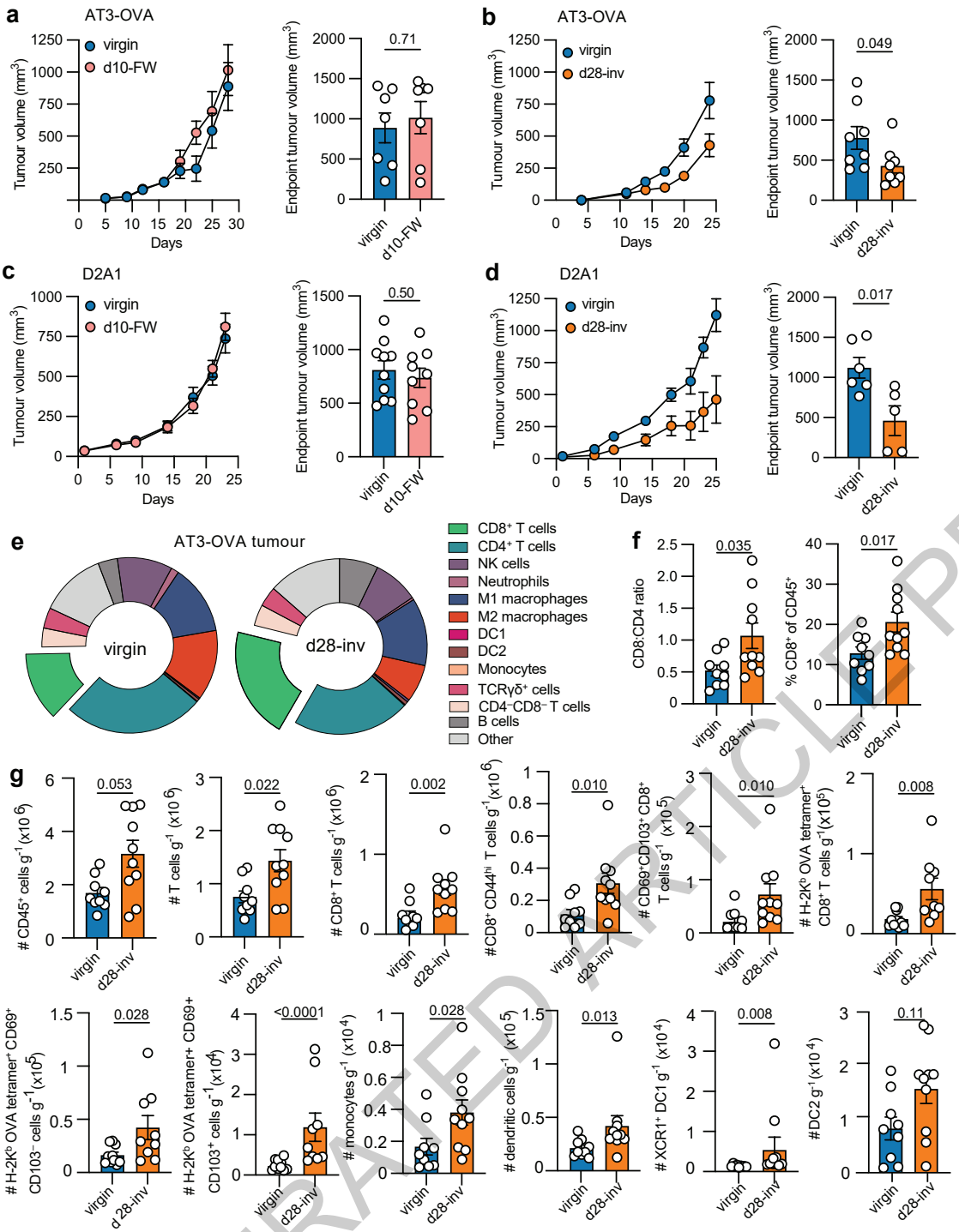

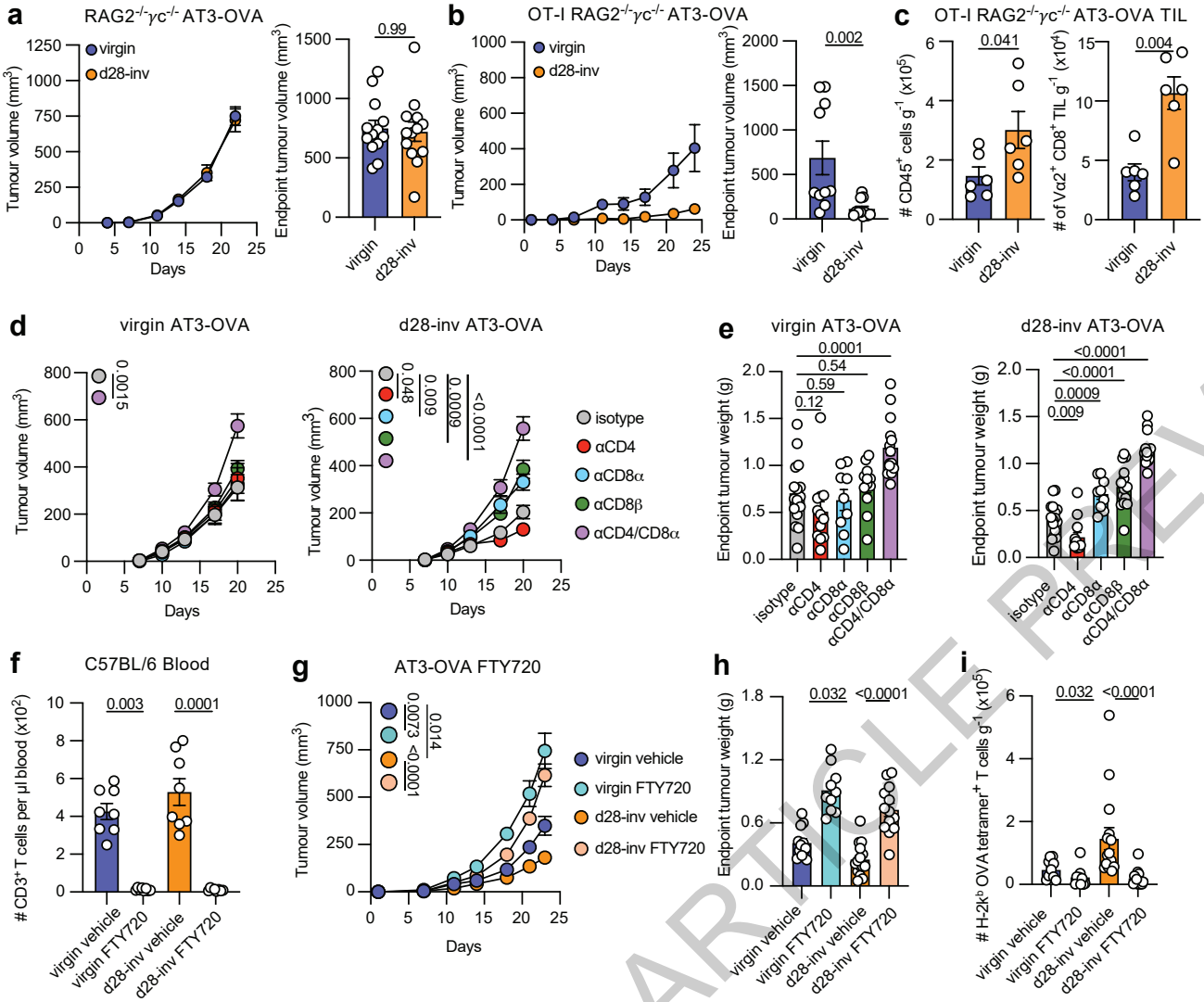

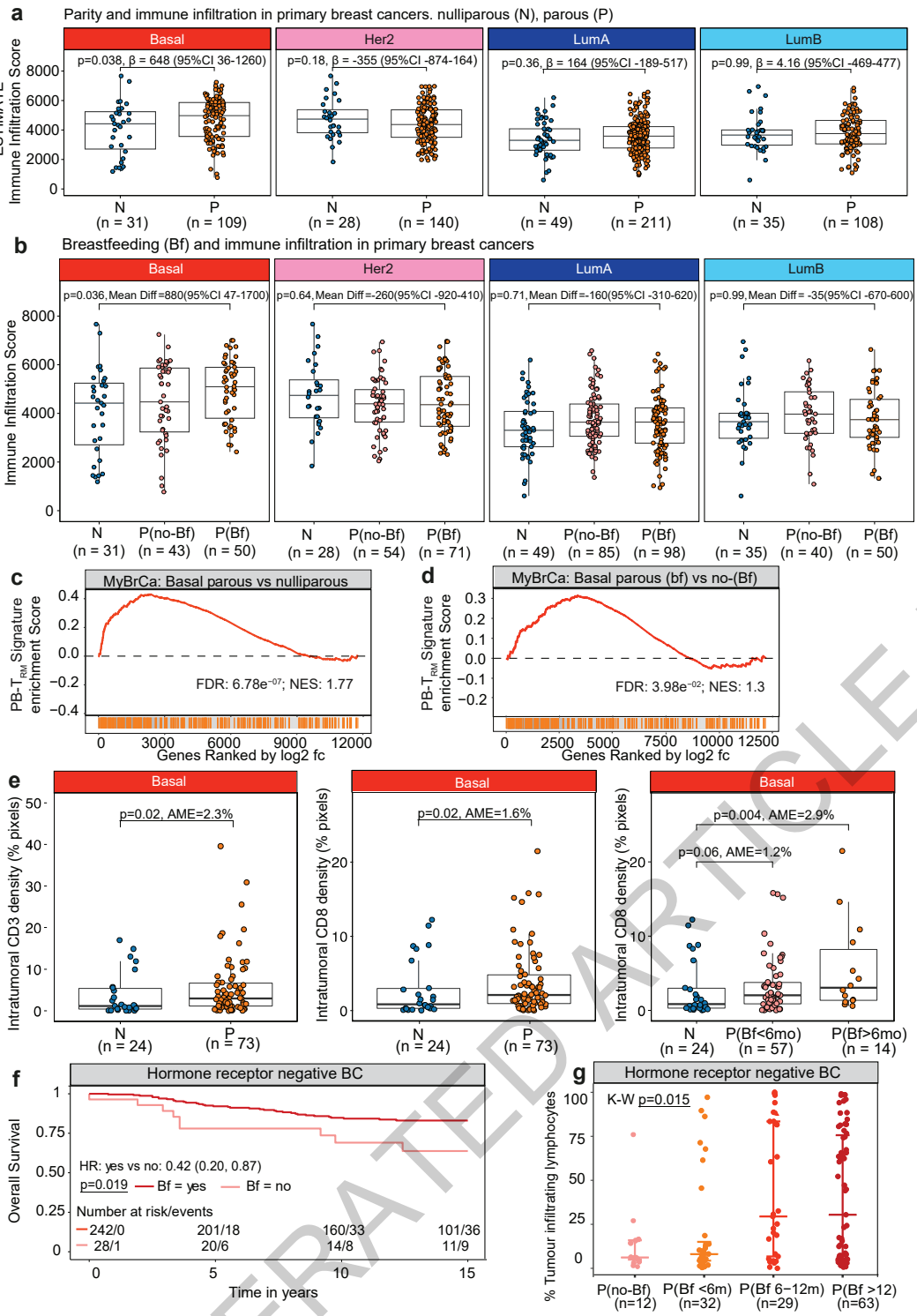

Extended Data Figure 1

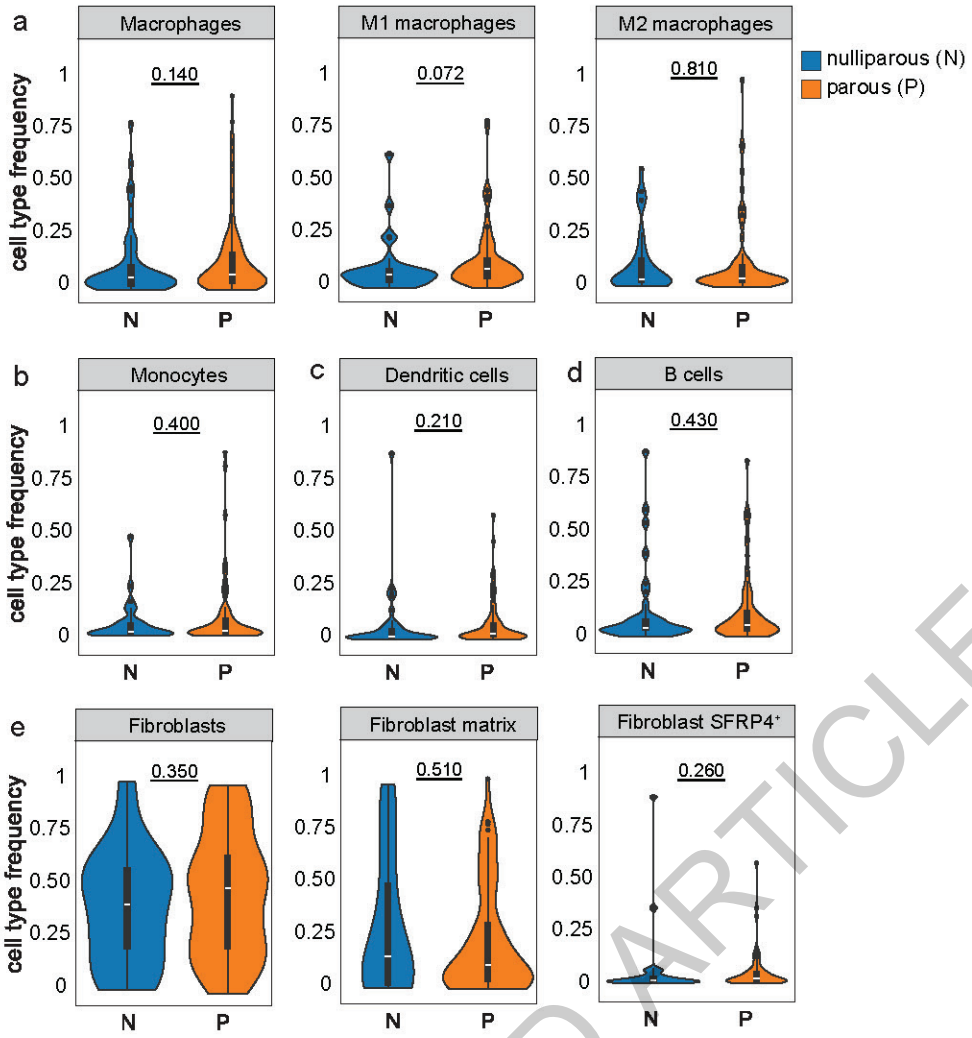

Extended Data Figure 2

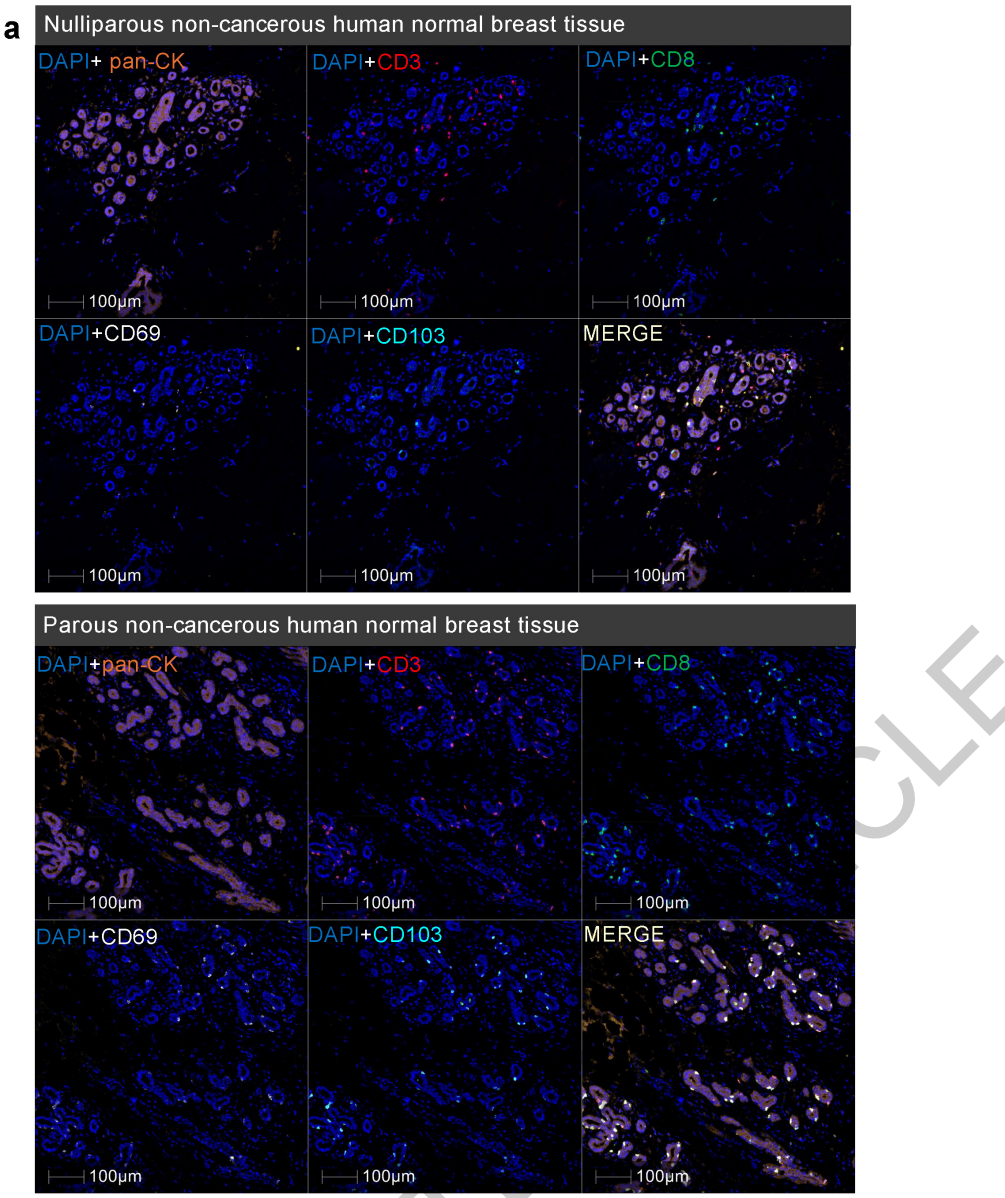

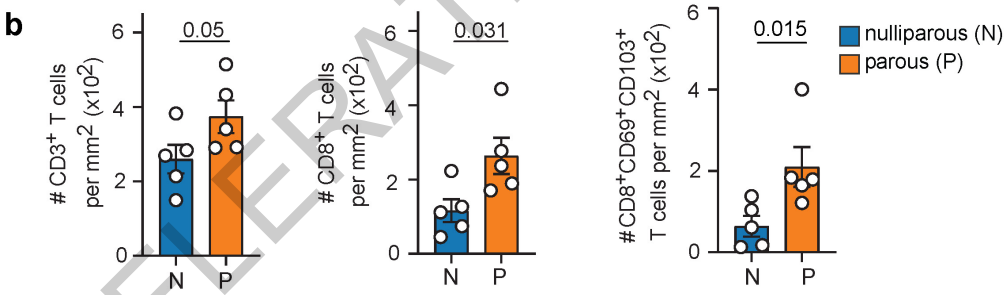

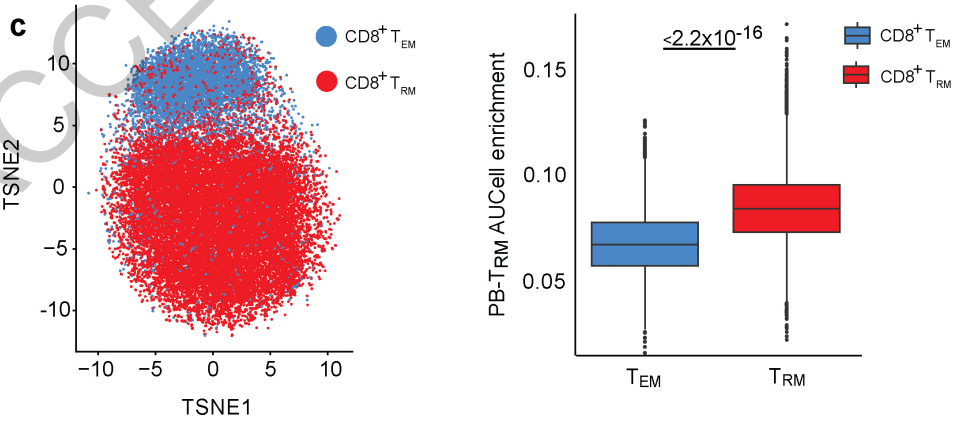

Extended Data Figure 3

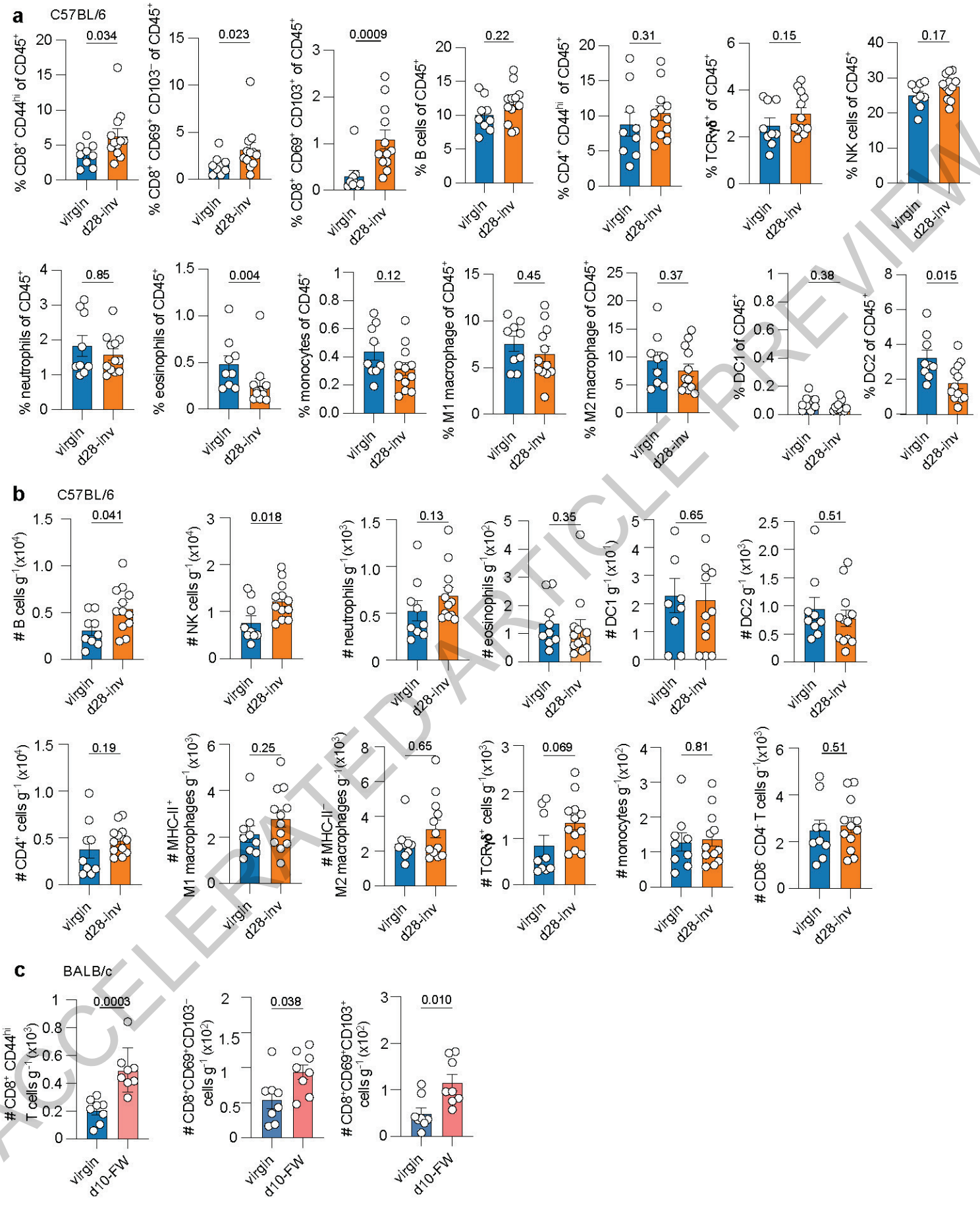

Extended Data Figure 4

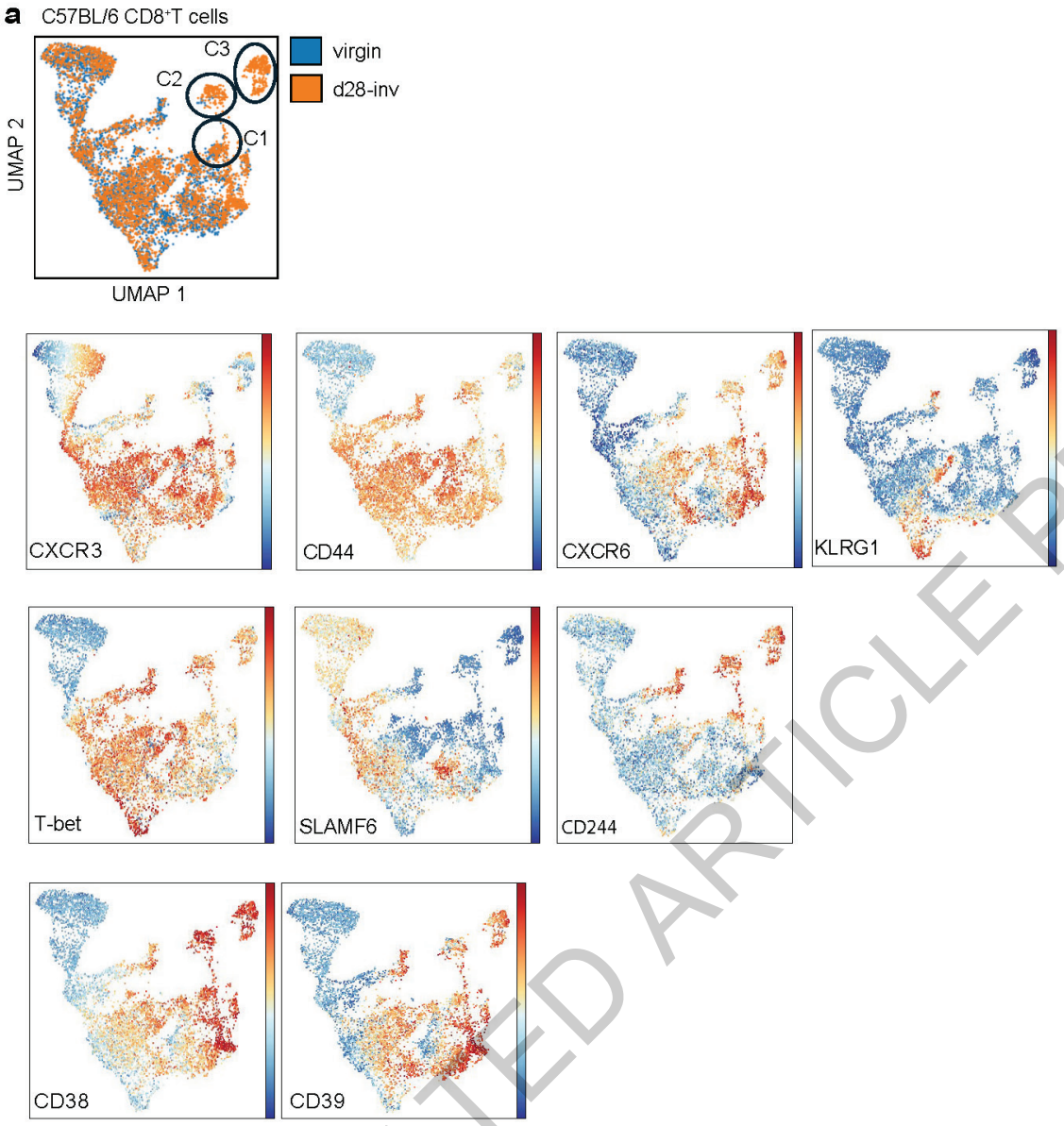

Extended Data Figure 5

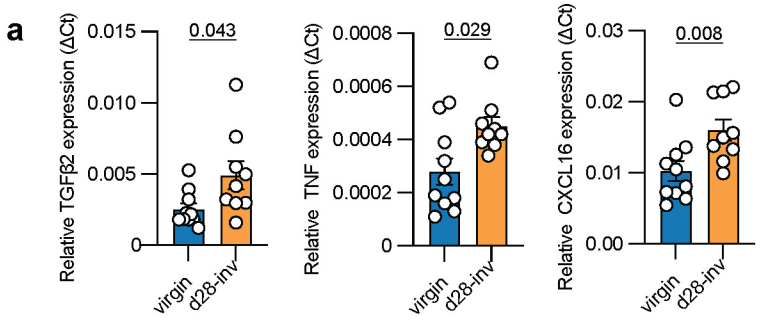

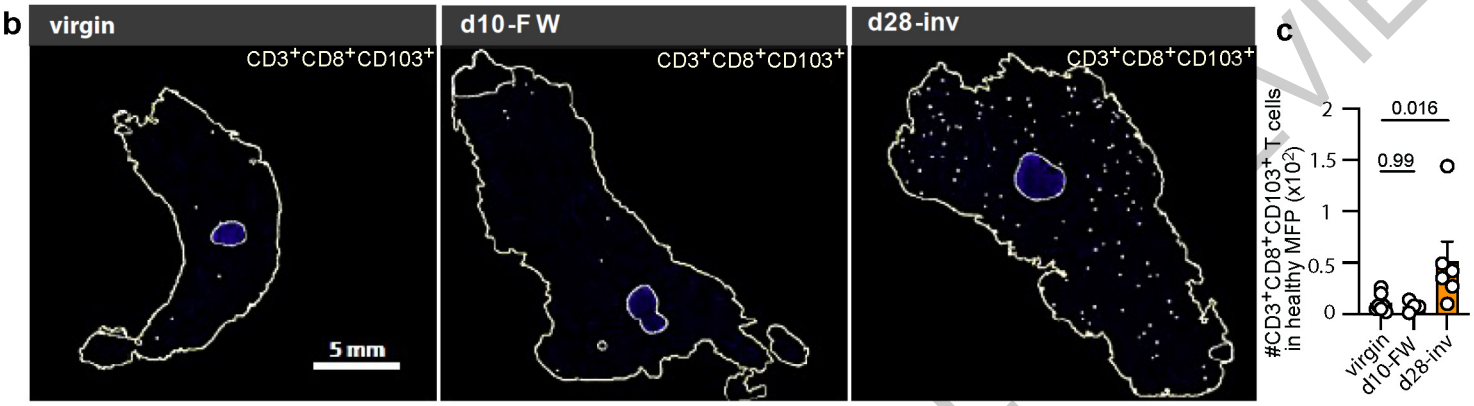

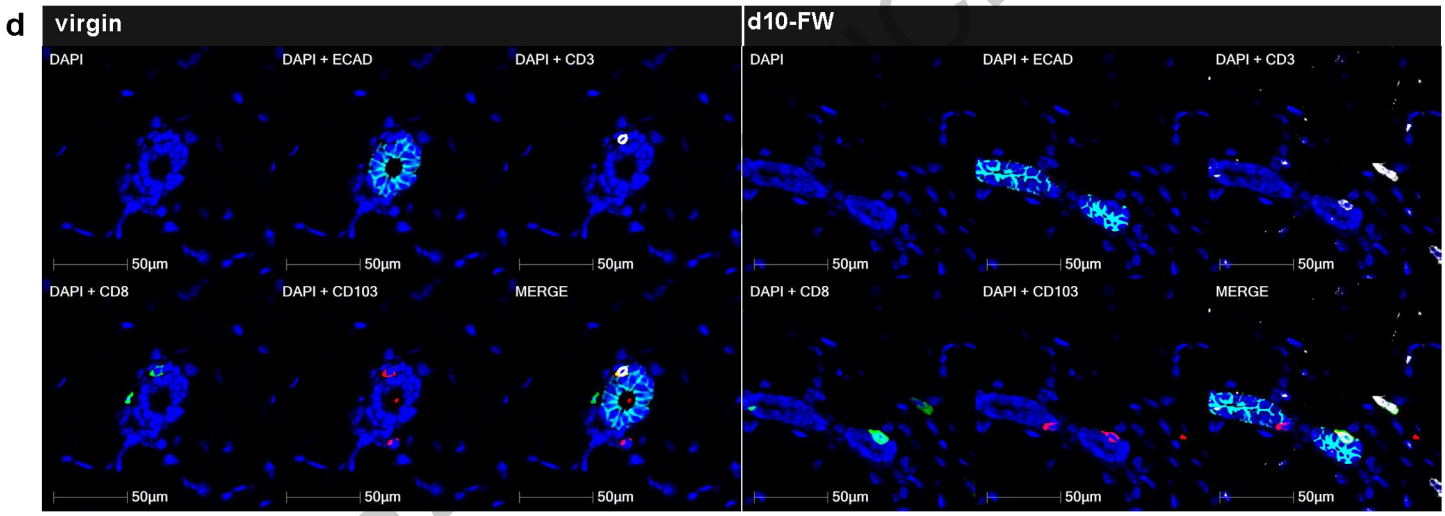

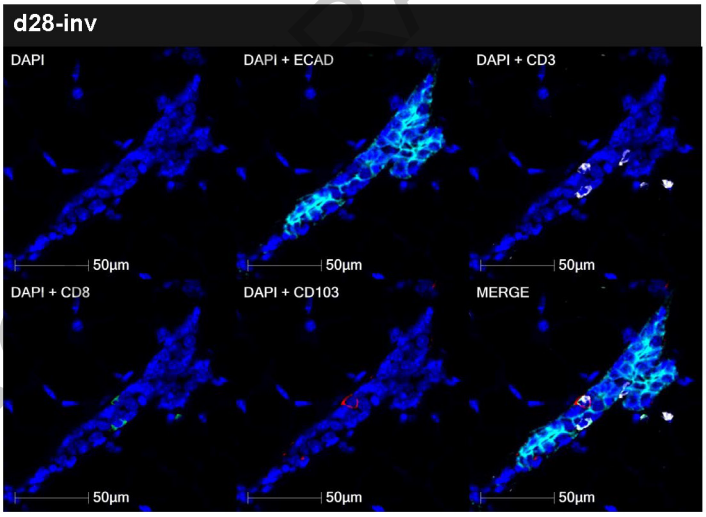

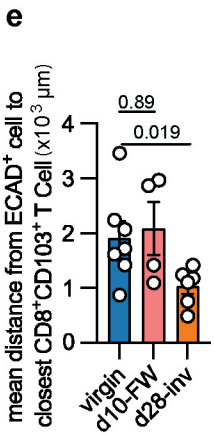

Extended Data Figure 6

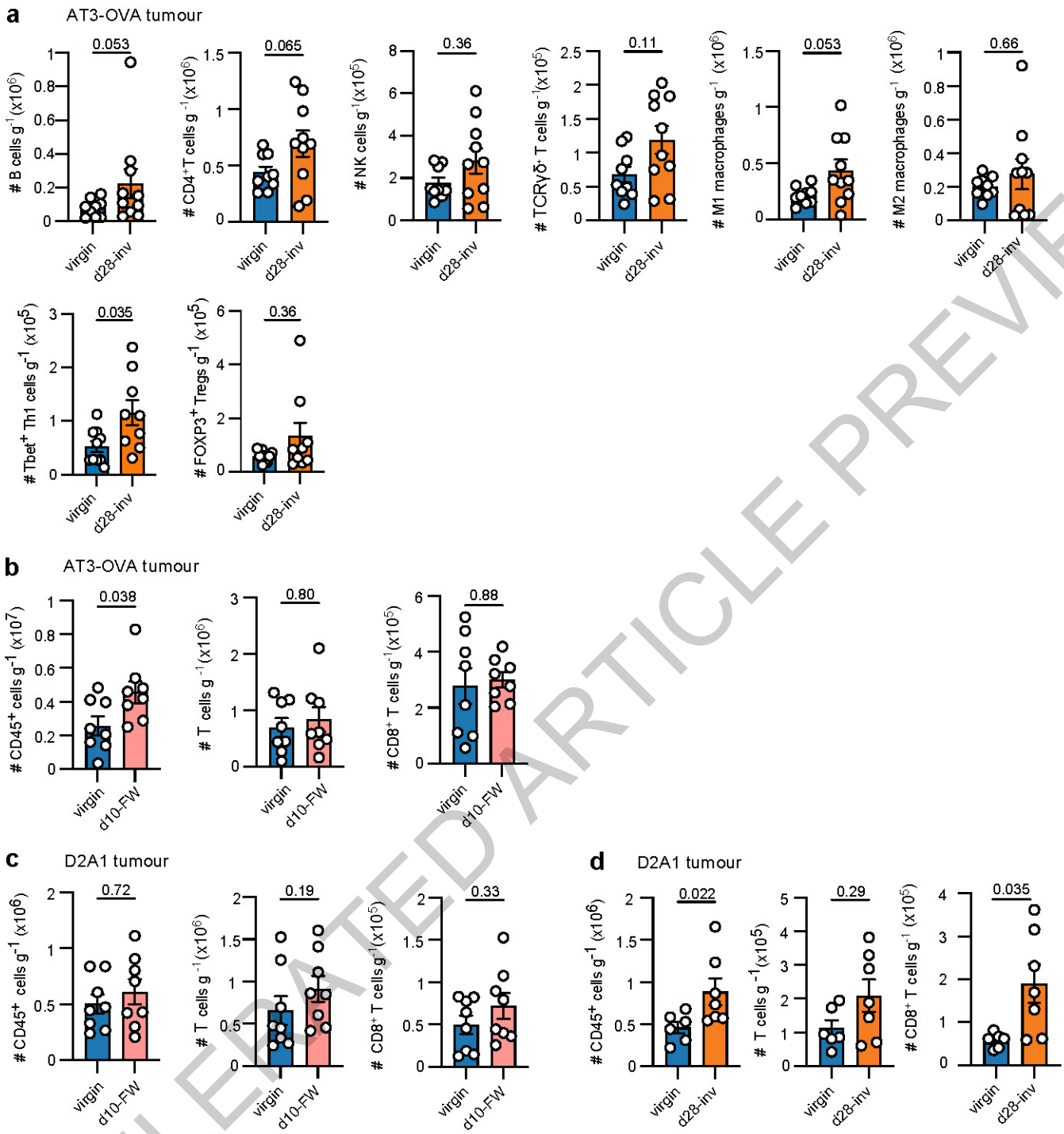

Extended Data Figure 7

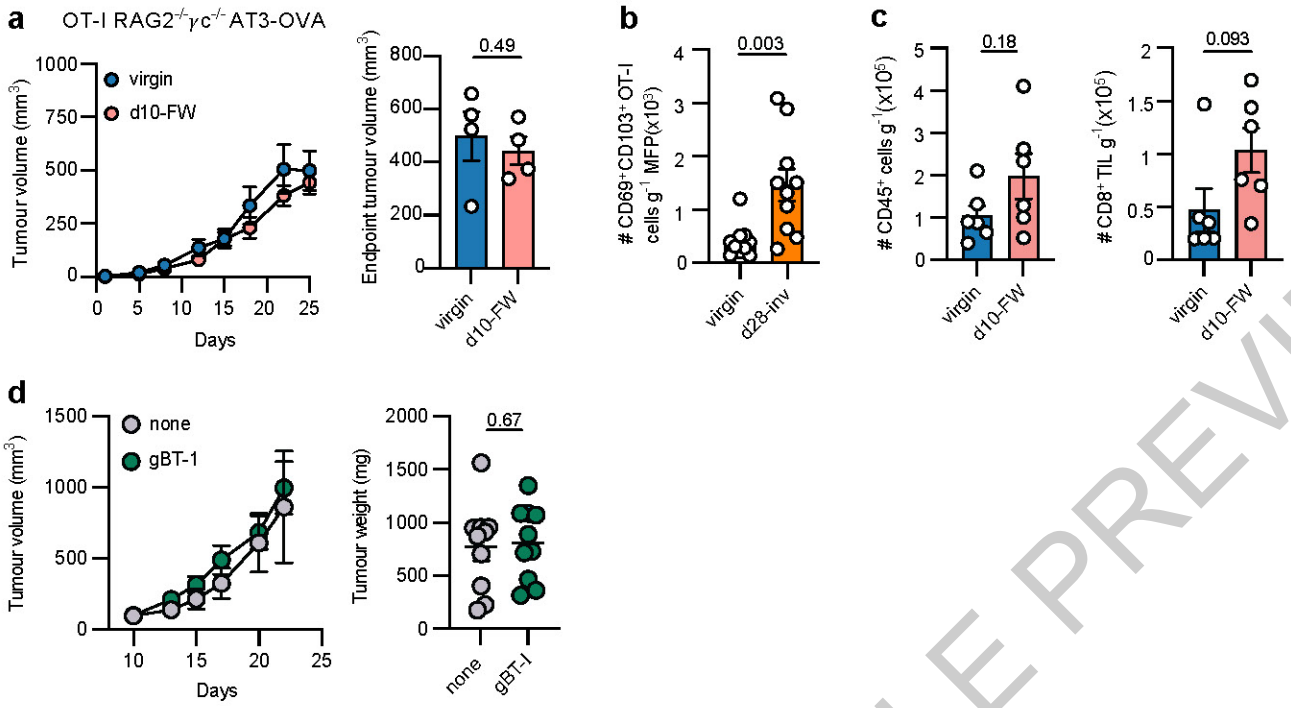

Extended Data Figure 8

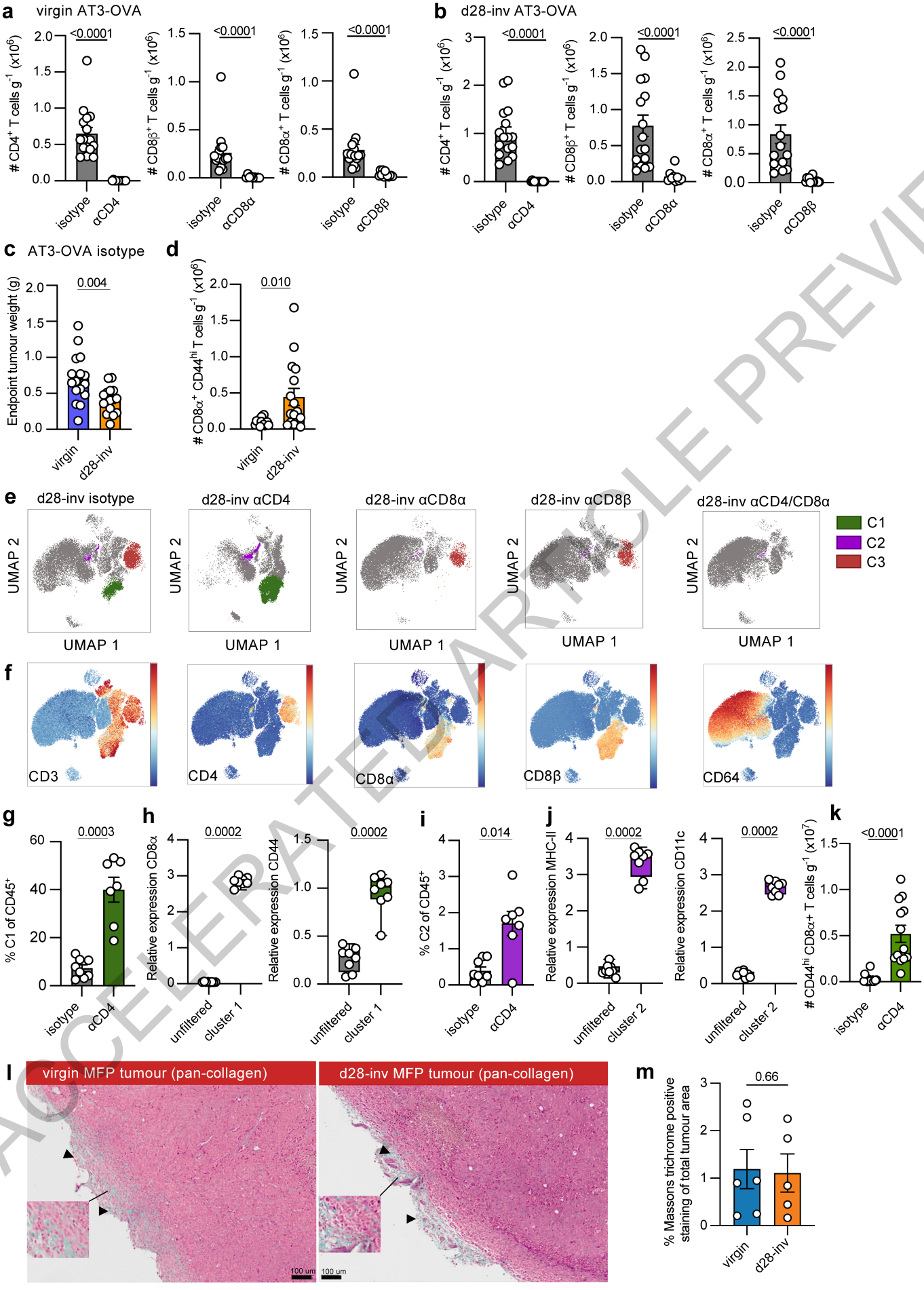

Extended data Figure 9

a

Variable		N	Hazard ratio	Confidence intervals	p value
breastfeeding	no	28		Reference	
	yes	242		0.39 (0.19, 0.79)	0.009
age at diagnosis		270		1.04 (0.99, 1.09)	0.083
time since last birth	≤10	122		Reference	
	>10	148		0.45 (0.19, 1.06)	0.066
treatment chemo	no	80		Reference	
	yes	190		1.47 (0.75, 2.87)	0.258
treatment mastectomy	no	66		Reference	
	yes	204		0.53 (0.29, 0.98)	0.042

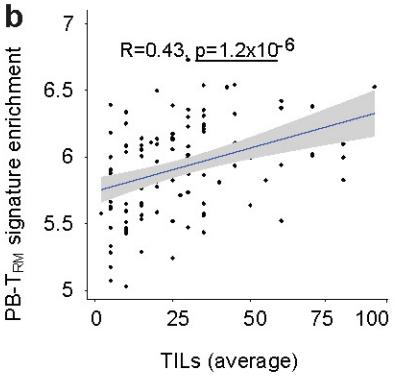

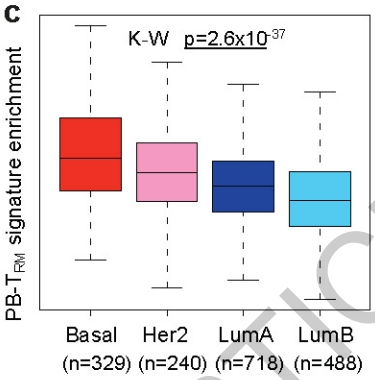

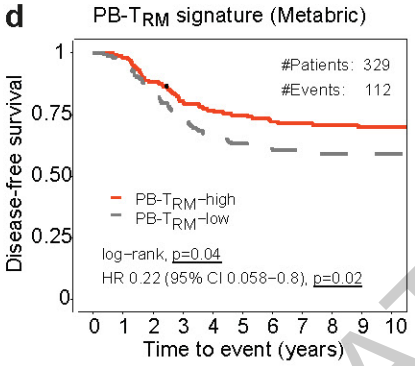

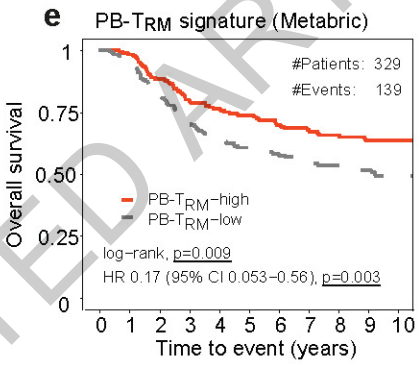

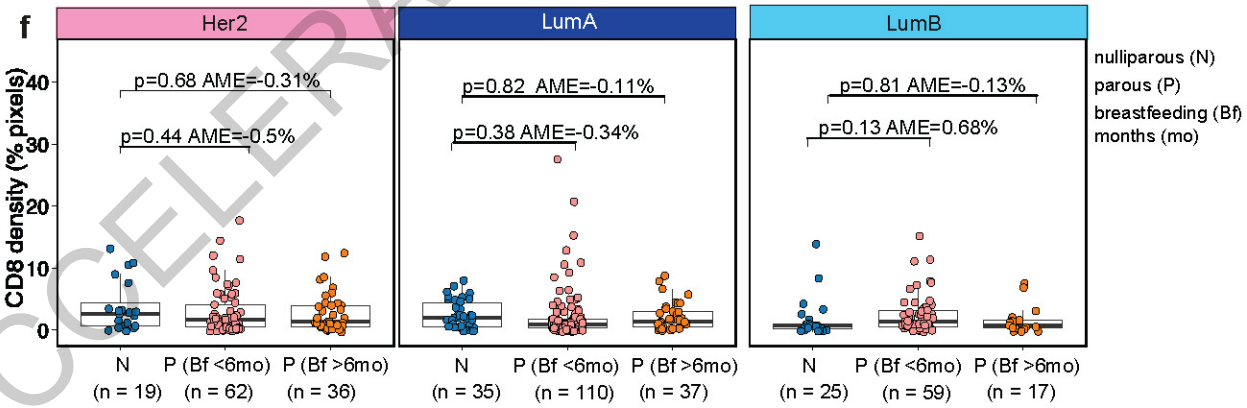

Extended Data Figure 10

a Flow cytometry gating strategy for non-cancerous human normal breast tissue

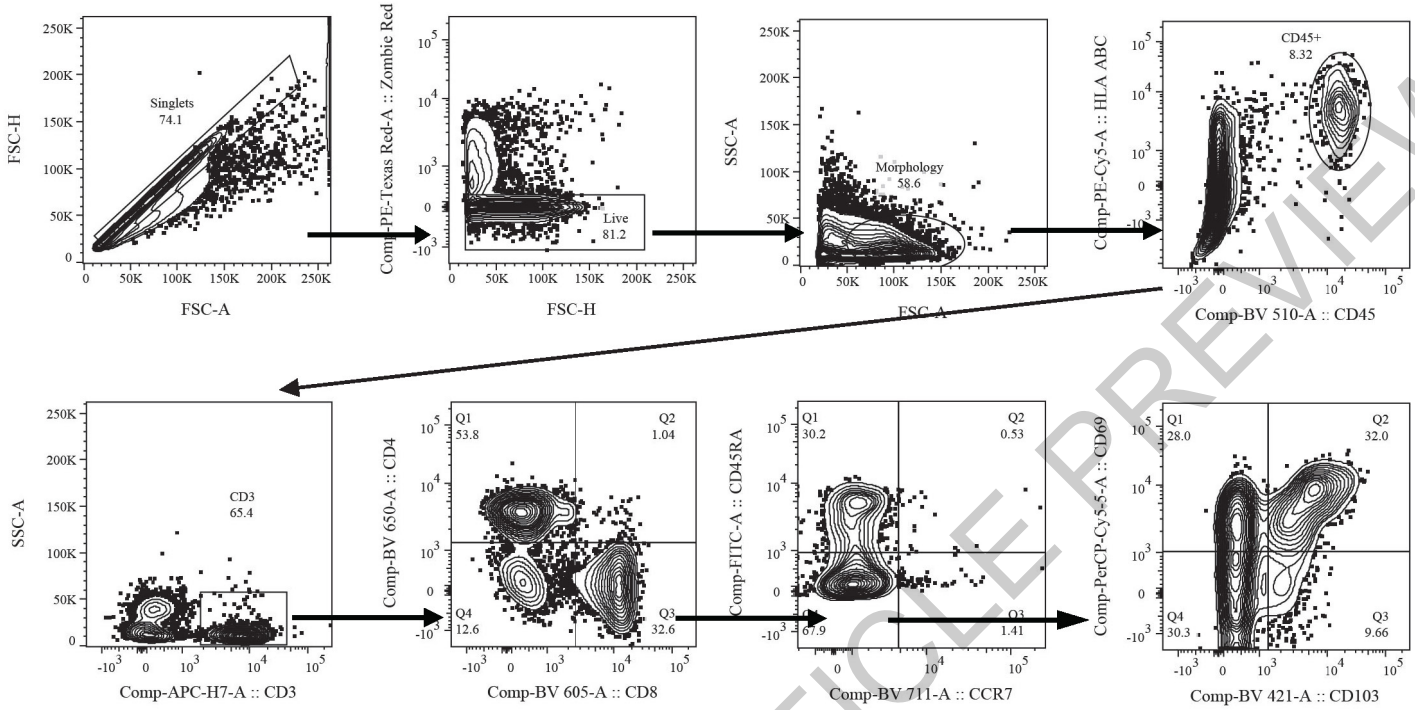

b Flow cytometry gating strategy for healthy murine mammary tissue

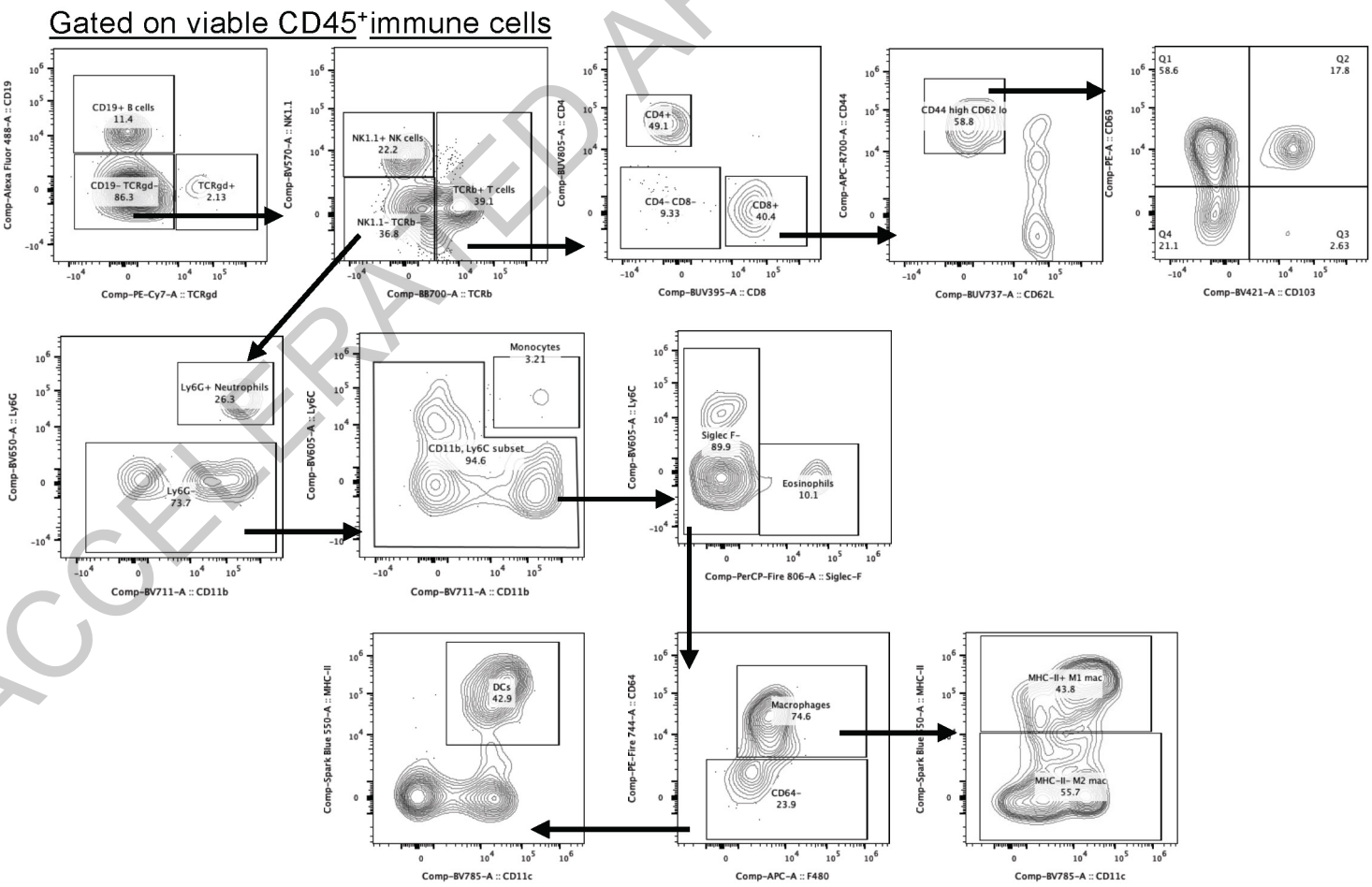

nature portfolio

Corresponding author(s): Prof. Sherene Loi and Prof. Laura K Mackay

Last updated by author(s): 17-09-2025

Reporting Summary

Nature Portfolio wishes to improve the reproducibility of the work that we publish. This form provides structure for consistency and transparency in reporting. For further information on Nature Portfolio policies, see our Editorial Policies and the Editorial Policy Checklist.

Statistics

For all statistical analyses, confirm that the following items are present in the figure legend, table legend, main text, or Methods section.

n/a	Confirmed	
☐	☒	The exact sample size (*n*) for each experimental group/condition, given as a discrete number and unit of measurement
☐	☒	A statement on whether measurements were taken from distinct samples or whether the same sample was measured repeatedly
☐	☒	The statistical test(s) used AND whether they are one- or two-sided *Only common tests should be described solely by name; describe more complex techniques in the Methods section.*
☐	☒	A description of all covariates tested
☐	☒	A description of any assumptions or corrections, such as tests of normality and adjustment for multiple comparisons
☐	☒	A full description of the statistical parameters including central tendency (e.g. means) or other basic estimates (e.g. regression coefficient) AND variation (e.g. standard deviation) or associated estimates of uncertainty (e.g. confidence intervals)
☐	☒	For null hypothesis testing, the test statistic (e.g. *F*, *t*, *r*) with confidence intervals, effect sizes, degrees of freedom and *P* value noted *Give P values as exact values whenever suitable.*
☒	☐	For Bayesian analysis, information on the choice of priors and Markov chain Monte Carlo settings
☒	☐	For hierarchical and complex designs, identification of the appropriate level for tests and full reporting of outcomes
☐	☒	Estimates of effect sizes (e.g. Cohen's *d*, Pearson's *r*), indicating how they were calculated

Our web collection on statistics for biologists contains articles on many of the points above.

Software and code

Policy information about availability of computer code

Data collection	Flow cytometry, FlowJo v10 (FlowJo LLC). R analyses, ggeffects (v2.2.1), betareg (v3.2-1), AUCell (v1.28.0) AME margin (v0.3.28),RUV-III (v0.9.7.1),limma (v3.60.3),fgsea (v1.30.0),Harmony (v1.2.3),Seurat (v5.2.1),confint' (v1.11.0), dplyr 1.1.2, tidyr 1.3.0, readxl 1.4.3, readr 2.1.4 and magrittr 2.0.3.Sequencing, HTSeq (v2.0.3), Microscopy,HALO v3.6.4134 and HighPlex FL v4.2.3.
Data analysis	FlowJo version 10 (FlowJo LLC), DE gene analysis performed using R limma (v3.60.3). Volcano plots with ggplot2 (v3.5.1).Statistical analysis and data presentation: Graphpad Prism 9, GSEA analysis derived from GSE112825 Santucci et al 2019.statistical analyses for human cohort were conducted using Rv4 and murine cohort data analyses using Graphpad Prism v9, General: Microsoft Excel 2010

For manuscripts utilizing custom algorithms or software that are central to the research but not yet described in published literature, software must be made available to editors and reviewers. We strongly encourage code deposition in a community repository (e.g. GitHub). See the Nature Portfolio guidelines for submitting code & software for further information.

Data

Policy information about availability of data

All manuscripts must include a data availability statement. This statement should provide the following information, where applicable:

- Accession codes, unique identifiers, or web links for publicly available datasets
- A description of any restrictions on data availability
- For clinical datasets or third party data, please ensure that the statement adheres to our policy

Processed and raw RNA Sequencing counts for human PB-TRM signature can be accessed via publicly available GEO: GSE271307 and Data availability statement has been provided in the manuscript including accession codes.

Research involving human participants, their data, or biological material

Policy information about studies with human participants or human data. See also policy information about sex, gender (identity/presentation), and sexual orientation and race, ethnicity and racism.

Reporting on sex and gender	"Parity and lactation induce T cell mediated breast cancer protection" only apply to women.
Reporting on race, ethnicity, or other socially relevant groupings	Malaysian and Australian (European ancestry predominantly) cohorts (Figure 5) Reed et al. collated datasets in Figure 1a also including European, Hispanic , Asian, African American populations.
Population characteristics	Demographic (patients de-identified) information were provided in SI table guide from Kathleen Cuningham Foundation Consortium for Research into Familial Breast Cancer (kConFab), Australia.
Recruitment	For Breast FACS and TILs/breastfeeding analyses, patients were approached by a prospective biobanking effort prior to commencement of this study. No significant biases are expected. Human MyBrCa cohort was a large study designed to recruit broadly. Again no important biases expected.
Ethics oversight	Complete ethics information and approval numbers for human and murine studies are provided in the manuscript methods section.

Note that full information on the approval of the study protocol must also be provided in the manuscript.

Field-specific reporting

Please select the one below that is the best fit for your research. If you are not sure, read the appropriate sections before making your selection.

☒ Life sciences ☐ Behavioural & social sciences ☐ Ecological, evolutionary & environmental sciences

For a reference copy of the document with all sections, see nature.com/documents/nr-reporting-summary-flat.pdf

Life sciences study design

All studies must disclose on these points even when the disclosure is negative.

Sample size	In an exploratory study of this nature it is not possible to pre-specify the sample size. Cases were acquired, data analyzed and demographic and information surrounding epidemiology were gathered retrospectively at the final endpoint post collation of full comprehensive analsysis. The final sample size was determined in an adaptive fashion based on equal representation.
Data exclusions	MyBrCa clinical cohort, 3 cases without PAM50, 20 cases contained “normal-like” classification were excluded from the analysis. Parity was defined as at least one live birth, and pregnancy-associated cancers were not excluded in this analysis.
Replication	All characterisations of breast immune infiltration were replicated in 90 patient cohort as described in respective methods sections and Bulk RNASeq was performed on T cells isolated from multiple cases and matched peripheral blood contrasts were used for comparison. Mammary infiltrating lymphocytes in murine models shown by flow cytometry, immunohistochemistry, tumour models were replicated at least twice, shown from either pooled repeats or representative of independent repeats with similar results indicated in figure legends
Randomization	Therapeutic interventions in murine studies begun prior tumour cell inoculation and continued following BC onset randomization is not relevant.
Blinding	Investigators performed prospective collections for human and murine cohorts, retrosective analyses were performed from published datasets Data was not blinded.

Reporting for specific materials, systems and methods

We require information from authors about some types of materials, experimental systems and methods used in many studies. Here, indicate whether each material, system or method listed is relevant to your study. If you are not sure if a list item applies to your research, read the appropriate section before selecting a response.

Materials & experimental systems

n/a	Involved in the study
☐	☒ Antibodies
☐	☒ Eukaryotic cell lines
☒	☐ Palaeontology and archaeology
☐	☒ Animals and other organisms
☒	☐ Clinical data
☒	☐ Dual use research of concern
☒	☐ Plants

Methods

n/a	Involved in the study
☒	☐ ChIP-seq
☐	☒ Flow cytometry
☒	☐ MRI-based neuroimaging

Antibodies

Antibodies used

Human antibodies:
Marker; Flurophore; Catalogue#, Supplier
CD45 BV510 Human 304036 B2411217 H130 Biolegend
CD45 FITC Human 555482 4248832 H130 BD Biosciences
CD3 APC-H7 Human 560176 7234624 SK7 BD Biosciences
CD8 BV605 Human 301040 B230656 RPA-T8 Biolegend
CD8 PE Human 555635 6095935 HIT8a BD Biosciences
CD4 BV650 Human 317436 B2300991 OKT4 Biolegend
CD197,CCR7 BV711 Human 353228 B223097 G043H7 Biolegend
CD45RA FITC Human 555488 5181589 HI100 BD Biosciences CD69 PerCP-Cy5.5 Human 310926 B234158 FN50 Biolegend HLA ABC PE-Cy5 Human 555554 5163888 G46-2.6 BD
CD69 PECY7 Human 310912 B210943 FN50 Biolegend
CD103 BV421 Human 350214 B238177 BerACT8 Biolegend pan-cytokeratin (AE1/AE3); Human ;M3515; DAKO
CD3e;(SP7); Human; Ab16669;Abcam
CD8;(4B11); Human; NCL-L-CD8-4B11;Leica Biosystems CD69; (EPR21814);Human;Ab233396; Abcam
CD103;(EPR416602);Human;Ab129202; Abcam

Murine antibodies
CD45 APCCY7;Mouse; 109824;Biolegend
TCR-β BB700 Mouse; 745846 BD Biosciences
TCR-β BV786 Mouse 742484 Biosciences
TCR-Vα2 PerCP Cy5.5 Mouse 560529 BD Pharmagen
CD8 BV711 Mouse 100748 Biolegend
CD8 BUV395 Mouse 563786 BD Pharmagen
CD4 BUV805 Mouse 741912 BD Pharmagen
CD44 BV605 Mouse 103047 Biolegend
CD62L PECY7 Mouse 104418 Biolegend
CD62L BUV737 Mouse 612833 Pharmagen
CD69 BUV395 Mouse 38290563760 BD Pharmagen
CD69 PE Mouse 12069183 Invitrogen
CD103 FITC Mouse 121420 Biolegend
CD103 PE Mouse 12103182 Invitrogen
CD11B BV711 Mouse 101242 Biolegend
CD11C BV786 Mouse 117335 Biolegend
F4/80 EF-450 Mouse 48480182 Invitrogen
MHC-II (I-A/I-E) APC Mouse 17532182 Invitrogen
CD1d tetramer biotinylated PBS-57 66233 NIH
Streptavidin PE Mouse 12-4317-87 eBioscience
Streptavidin PE Mouse 554061 BD Pharmagen
BioxCell murine depletion antibodies; Isotype control rat IgG2b catalogue #BE0090;Anti-CD4 clone GK1.5, catalogue # BE0003-1;Anti-CD8a clone YTS 169.4, catalogue # BE0117; Anti-CD8b clone 53-5.8, catalogue # BE0223.

Murine antibodies

Marker	Fluorphore	Catalogue #	Supplier
CD49a	BUV395	740262	BD
NK1.1	BUV563	741233	BD
CD8b	BUV661	741585	BD
CD8a	RB545	569278	BD
CD4	BUV805	741913	BD
Ly108	BV421	740090	BD
CD103	BV480	566118	BD
CD44	BV510	563114	BD
Ly6C	BV570	128030	Biolegend
KLRG1	BV605	564013	Biolegend
CXCR3	BV650	126531	Biolegend
CD39	BV711	567295	BD
PD-1	BV750	135263	Biolegend
CD244	BV785	740860	BD
TCRgd	BB700	745818	BD
CXCR6	PE-Dazzle54	151117	Biolegend
CD69	PE-Cy5	15-0691-82	Invitrogen
CD45.2	SparkNIR685	109864	Biolegend
CD62L	APC-R700	565159	BD
TCRb	APC-Cy7	109220	Biolegend
CD38	APC-Fire810	102746	Biolegend
Granzyme A	ef450	3029841	Invitrogen
TCF1	AF488	644S	CST
Granzyme B	APC	MHGB05	Invitrogen
Tbet	PE/Fire 810	644839	Biolegend
CD45	PerCP	103130	Biolegend
CD19	AF488	115521	Biolegend
TCRgd	PE-Cy7	118123	Biolegend
NK1.1	BV570	108733	Biolegend
CD3	SparkNIR685	100262	Biolegend
CD44	APCR700	565480	BD
CD62L	BUV737	612833	BD
CD103	BV421	121422	Biolegend
CD49a	BUV563	741306	BD
CD39	PE-Dazzle 594	143812	Biolegend
CD11b	BV711	209715	Biolegend
CD11c	BV785	117335	Biolegend
F480	APC	123115	Biolegend
Ly6G	BV650	127641	Biolegend
Ly6C	BV605	128036	Biolegend
MHC-II	SparkBlue550	107661	Biolegend
CD170	PerCP-Fire 806	155536	Biolegend
XCR1	Spark UV387	148236	Biolegend
SIRPa	APC-Fire750	144030	Biolegend
CX3CR1	Spark Blue 574	285185	Biolegend
CD64	PE-Fire 744	161010	BD
PD1	RY586	753854	BD
FOXP3	e450	48-5773-82	Thermofisher

Validation

All antibodies were validated by the supplier and validation statements are available in the manufacturer's website. Additionally, functional experiments were reported in extended figures for murine T cell depletion antibodies provided in the manuscript.

Eukaryotic cell lines

Policy information about cell lines and Sex and Gender in Research

Cell line source(s)	AT3-OVA and D2A1 cell lines sourced from Prof. Phil Darcy and A/Prof Kara Britt respectively from Peter MacCallum Cancer Centre laboratory stocks, Melbourne, Australia
Authentication	Both cell lines were well established and published.
Mycoplasma contamination	Cell lines in this study were repetitively tested mycoplasma negative.
Commonly misidentified lines (See ICLAC register)	Cell lines in this study are not listed in the ILAC database.

Animals and other research organisms

Policy information about studies involving animals; ARRIVE guidelines recommended for reporting animal research, and Sex and Gender in Research

Laboratory animals	C57BL/6J wild type (wt) and BALB/c wt mice, RAG1-/-; RAG2-/-γc-/- and OT-I CD45.2 and gBT-I CD45.1/CD45.2.Mice were used between 7-8 weeks of age.
Wild animals	no wild animals were used in the study.
Reporting on sex	female mice
Field-collected samples	This study does not involve samples collected from the field
Ethics oversight	All animal experiments procedures conducted in this study were approved by the relevant Peter MacCallum Cancer Centre Animal Experimentation Ethics Committee or by The University of Melbourne Animal Ethics Committee and conducted in accordance with the National Health and Medical Research Council Australian Code of Practice for the Care and Use of Animals for Scientific Purposes.

Note that full information on the approval of the study protocol must also be provided in the manuscript.

Clinical data

Policy information about clinical studies

All manuscripts should comply with the ICMJE guidelines for publication of clinical research and a completed CONSORT checklist must be included with all submissions.

Clinical trial registration	We utilised immune scores and associated clinical information from the MyBrCa dataset obtained from the original publication that contain BC subtype, parity information and breastfeeding data were described Pan et al 2024. This was not a clinical trial
Study protocol	Clinical data previously reported in Pan ***et al*** 2024
Data collection	Extended MyBrCa demo table were provided in the supplemental table information in the current study and were previously described in Pan ***et al*** 2024.
Outcomes	Clinical data reported in Pan et al 2024. In this study we utilized report significantly higher tumoural immune content in “basal-like” TNBC in parous women overall, compared with the Nulliparous women who subsequently developed breast cancer and our parous (PB)-TRM gene signature was highly enriched with both parity and breastfeeding status, highlighting the specificity of the P-TRM signature to breast involution by parity, and the specific influence of lactation.

Plants

Seed stocks	not applicable
Novel plant genotypes	not applicable
Authentication	not applicable

Flow Cytometry

Plots

Confirm that:

☒ The axis labels state the marker and fluorochrome used (e.g. CD4-FITC).

☒ The axis scales are clearly visible. Include numbers along axes only for bottom left plot of group (a 'group' is an analysis of identical markers).

☒ All plots are contour plots with outliers or pseudocolor plots.

☒ A numerical value for number of cells or percentage (with statistics) is provided.

Methodology

Sample preparation	Human breast and Murine tissue samples were dissociated into single cell suspension was created using a modified published protocol Savas et al 2018. Adipose content were removed briefly from the mammary glands and the connective tissues were then finely diced into smaller fragments in RPMI1640 containing, 1 mg/ml collagenase type 4 and incubated for 30 minutes at 37C. Digested tissue fragments were teased through a 70um sieve, the sieve irrigated with neat PBS prior downstream analyses (Please refer further to respective tissue processing methods and resources table)
Instrument	BD Symphony A5 or LSR Fortessa X-20 (BD Biosciences, San Diego, CA, USA); 5-laser Cytek Aurora (Cytek Biosciences)
Software	FlowJo Version 10; OMIQ were used for FACS data interpretation and data presentation
Cell population abundance	Bulk RNA Seq, a total of 5x10e3 and blood 1x10e4 T cell fractions were FACS purified. Reanalysis of isolated CD8+ T cell following FACS were assessed for >90% purity of individual samples. total immune counts per gram were presented.
Gating strategy	Gating strategies including preliminary FSC/SSC gates of the starting population were provided **in Extended Data Figure 11 legends**

☒ Tick this box to confirm that a figure exemplifying the gating strategy is provided in the Supplementary Information.

nature portfolio

Corresponding author(s): Prof. Sherene Loi and Prof. Laura K Mackay

Last updated by author(s): 17-09-2025

Reporting Summary

Nature Portfolio wishes to improve the reproducibility of the work that we publish. This form provides structure for consistency and transparency in reporting. For further information on Nature Portfolio policies, see our Editorial Policies and the Editorial Policy Checklist.

Statistics

For all statistical analyses, confirm that the following items are present in the figure legend, table legend, main text, or Methods section.

n/a	Confirmed	
☐	☒	The exact sample size (*n*) for each experimental group/condition, given as a discrete number and unit of measurement
☐	☒	A statement on whether measurements were taken from distinct samples or whether the same sample was measured repeatedly
☐	☒	The statistical test(s) used AND whether they are one- or two-sided *Only common tests should be described solely by name; describe more complex techniques in the Methods section.*
☐	☒	A description of all covariates tested
☐	☒	A description of any assumptions or corrections, such as tests of normality and adjustment for multiple comparisons
☐	☒	A full description of the statistical parameters including central tendency (e.g. means) or other basic estimates (e.g. regression coefficient) AND variation (e.g. standard deviation) or associated estimates of uncertainty (e.g. confidence intervals)
☐	☒	For null hypothesis testing, the test statistic (e.g. *F*, *t*, *r*) with confidence intervals, effect sizes, degrees of freedom and *P* value noted *Give P values as exact values whenever suitable.*
☒	☐	For Bayesian analysis, information on the choice of priors and Markov chain Monte Carlo settings
☒	☐	For hierarchical and complex designs, identification of the appropriate level for tests and full reporting of outcomes
☐	☒	Estimates of effect sizes (e.g. Cohen's *d*, Pearson's *r*), indicating how they were calculated

Our web collection on statistics for biologists contains articles on many of the points above.

Software and code

Policy information about availability of computer code

Data collection	Flow cytometry, FlowJo v10 (FlowJo LLC). R analyses, ggeffects (v2.2.1), betareg (v3.2-1), AUCell (v1.28.0) AME margin (v0.3.28),RUV-III (v0.9.7.1),limma (v3.60.3),fgsea (v1.30.0),Harmony (v1.2.3),Seurat (v5.2.1),confint' (v1.11.0), dplyr 1.1.2, tidyr 1.3.0, readxl 1.4.3, readr 2.1.4 and magrittr 2.0.3.Sequencing, HTSeq (v2.0.3), Microscopy,HALO v3.6.4134 and HighPlex FL v4.2.3.
Data analysis	FlowJo version 10 (FlowJo LLC), DE gene analysis performed using R limma (v3.60.3). Volcano plots with ggplot2 (v3.5.1).Statistical analysis and data presentation: Graphpad Prism 9, GSEA analysis derived from GSE112825 Santucci et al 2019.statistical analyses for human cohort were conducted using Rv4 and murine cohort data analyses using Graphpad Prism v9, General: Microsoft Excel 2010

For manuscripts utilizing custom algorithms or software that are central to the research but not yet described in published literature, software must be made available to editors and reviewers. We strongly encourage code deposition in a community repository (e.g. GitHub). See the Nature Portfolio guidelines for submitting code & software for further information.

Data

Policy information about availability of data

All manuscripts must include a data availability statement. This statement should provide the following information, where applicable:

- Accession codes, unique identifiers, or web links for publicly available datasets
- A description of any restrictions on data availability
- For clinical datasets or third party data, please ensure that the statement adheres to our policy

Processed and raw RNA Sequencing counts for human PB-TRM signature can be accessed via publicly available GEO: GSE271307 and Data availability statement has been provided in the manuscript including accession codes.

Research involving human participants, their data, or biological material

Policy information about studies with human participants or human data. See also policy information about sex, gender (identity/presentation), and sexual orientation and race, ethnicity and racism.

Reporting on sex and gender	"Parity and lactation induce T cell mediated breast cancer protection" only apply to women.
Reporting on race, ethnicity, or other socially relevant groupings	Malaysian and Australian (European ancestry predominantly) cohorts (Figure 5) Reed et al. collated datasets in Figure 1a also including European, Hispanic , Asian, African American populations.
Population characteristics	Demographic (patients de-identified) information were provided in SI table guide from Kathleen Cuningham Foundation Consortium for Research into Familial Breast Cancer (kConFab), Australia.
Recruitment	For Breast FACS and TILs/breastfeeding analyses, patients were approached by a prospective biobanking effort prior to commencement of this study. No significant biases are expected. Human MyBrCa cohort was a large study designed to recruit broadly. Again no important biases expected.
Ethics oversight	Complete ethics information and approval numbers for human and murine studies are provided in the manuscript methods section.

Note that full information on the approval of the study protocol must also be provided in the manuscript.

Field-specific reporting

Please select the one below that is the best fit for your research. If you are not sure, read the appropriate sections before making your selection.

☒ Life sciences ☐ Behavioural & social sciences ☐ Ecological, evolutionary & environmental sciences

For a reference copy of the document with all sections, see nature.com/documents/nr-reporting-summary-flat.pdf

Life sciences study design

All studies must disclose on these points even when the disclosure is negative.

Sample size	In an exploratory study of this nature it is not possible to pre-specify the sample size. Cases were acquired, data analyzed and demographic and information surrounding epidemiology were gathered retrospectively at the final endpoint post collation of full comprehensive analsysis. The final sample size was determined in an adaptive fashion based on equal representation.
Data exclusions	MyBrCa clinical cohort, 3 cases without PAM50, 20 cases contained “normal-like” classification were excluded from the analysis. Parity was defined as at least one live birth, and pregnancy-associated cancers were not excluded in this analysis.
Replication	All characterisations of breast immune infiltration were replicated in 90 patient cohort as described in respective methods sections and Bulk RNASeq was performed on T cells isolated from multiple cases and matched peripheral blood contrasts were used for comparison. Mammary infiltrating lymphocytes in murine models shown by flow cytometry, immunohistochemistry, tumour models were replicated at least twice, shown from either pooled repeats or representative of independent repeats with similar results indicated in figure legends
Randomization	Therapeutic interventions in murine studies begun prior tumour cell inoculation and continued following BC onset randomization is not relevant.
Blinding	Investigators performed prospective collections for human and murine cohorts, retrosective analyses were performed from published datasets Data was not blinded.

Reporting for specific materials, systems and methods

We require information from authors about some types of materials, experimental systems and methods used in many studies. Here, indicate whether each material, system or method listed is relevant to your study. If you are not sure if a list item applies to your research, read the appropriate section before selecting a response.

Materials & experimental systems

n/a	Involved in the study
☐	☒ Antibodies
☐	☒ Eukaryotic cell lines
☒	☐ Palaeontology and archaeology
☐	☒ Animals and other organisms
☒	☐ Clinical data
☒	☐ Dual use research of concern
☒	☐ Plants

Methods

n/a	Involved in the study
☒	☐ ChIP-seq
☐	☒ Flow cytometry
☒	☐ MRI-based neuroimaging

Antibodies

Antibodies used

Human antibodies:
Marker; Flurophore; Catalogue#, Supplier
CD45 BV510 Human 304036 B2411217 H130 Biolegend
CD45 FITC Human 555482 4248832 H130 BD Biosciences
CD3 APC-H7 Human 560176 7234624 SK7 BD Biosciences
CD8 BV605 Human 301040 B230656 RPA-T8 Biolegend
CD8 PE Human 555635 6095935 HIT8a BD Biosciences
CD4 BV650 Human 317436 B2300991 OKT4 Biolegend
CD197,CCR7 BV711 Human 353228 B223097 G043H7 Biolegend
CD45RA FITC Human 555488 5181589 HI100 BD Biosciences CD69 PerCP-Cy5.5 Human 310926 B234158 FN50 Biolegend HLA ABC PE-Cy5 Human 555554 5163888 G46-2.6 BD
CD69 PECY7 Human 310912 B210943 FN50 Biolegend
CD103 BV421 Human 350214 B238177 BerACT8 Biolegend pan-cytokeratin (AE1/AE3); Human ;M3515; DAKO
CD3e;(SP7); Human; Ab16669;Abcam
CD8;(4B11); Human; NCL-L-CD8-4B11;Leica Biosystems CD69; (EPR21814);Human;Ab233396; Abcam
CD103;(EPR416602);Human;Ab129202; Abcam

Murine antibodies
CD45 APCCY7;Mouse; 109824;Biolegend
TCR-β BB700 Mouse; 745846 BD Biosciences
TCR-β BV786 Mouse 742484 Biosciences
TCR-Vα2 PerCP Cy5.5 Mouse 560529 BD Pharmagen
CD8 BV711 Mouse 100748 Biolegend
CD8 BUV395 Mouse 563786 BD Pharmagen
CD4 BUV805 Mouse 741912 BD Pharmagen
CD44 BV605 Mouse 103047 Biolegend
CD62L PECY7 Mouse 104418 Biolegend
CD62L BUV737 Mouse 612833 Pharmagen
CD69 BUV395 Mouse 38290563760 BD Pharmagen
CD69 PE Mouse 12069183 Invitrogen
CD103 FITC Mouse 121420 Biolegend
CD103 PE Mouse 12103182 Invitrogen
CD11B BV711 Mouse 101242 Biolegend
CD11C BV786 Mouse 117335 Biolegend
F4/80 EF-450 Mouse 48480182 Invitrogen
MHC-II (I-A/I-E) APC Mouse 17532182 Invitrogen
CD1d tetramer biotinylated PBS-57 66233 NIH
Streptavidin PE Mouse 12-4317-87 eBioscience
Streptavidin PE Mouse 554061 BD Pharmagen
BioxCell murine depletion antibodies; Isotype control rat IgG2b catalogue #BE0090;Anti-CD4 clone GK1.5, catalogue # BE0003-1;Anti-CD8a clone YTS 169.4, catalogue # BE0117; Anti-CD8b clone 53-5.8, catalogue # BE0223.

Murine antibodies

Marker	Fluorphore	Catalogue #	Supplier
CD49a	BUV395	740262	BD
NK1.1	BUV563	741233	BD
CD8b	BUV661	741585	BD
CD8a	RB545	569278	BD
CD4	BUV805	741913	BD
Ly108	BV421	740090	BD
CD103	BV480	566118	BD
CD44	BV510	563114	BD
Ly6C	BV570	128030	Biolegend
KLRG1	BV605	564013	Biolegend
CXCR3	BV650	126531	Biolegend
CD39	BV711	567295	BD
PD-1	BV750	135263	Biolegend
CD244	BV785	740860	BD
TCRgd	BB700	745818	BD
CXCR6	PE-Dazzle54	151117	Biolegend
CD69	PE-Cy5	15-0691-82	Invitrogen
CD45.2	SparkNIR685	109864	Biolegend
CD62L	APC-R700	565159	BD
TCRb	APC-Cy7	109220	Biolegend
CD38	APC-Fire810	102746	Biolegend
Granzyme A	ef450	3029841	Invitrogen
TCF1	AF488	644S	CST
Granzyme B	APC	MHGB05	Invitrogen
Tbet	PE/Fire 810	644839	Biolegend
CD45	PerCP	103130	Biolegend
CD19	AF488	115521	Biolegend
TCRgd	PE-Cy7	118123	Biolegend
NK1.1	BV570	108733	Biolegend
CD3	SparkNIR685	100262	Biolegend
CD44	APCR700	565480	BD
CD62L	BUV737	612833	BD
CD103	BV421	121422	Biolegend
CD49a	BUV563	741306	BD
CD39	PE-Dazzle 594	143812	Biolegend
CD11b	BV711	209715	Biolegend
CD11c	BV785	117335	Biolegend
F480	APC	123115	Biolegend
Ly6G	BV650	127641	Biolegend
Ly6C	BV605	128036	Biolegend
MHC-II	SparkBlue550	107661	Biolegend
CD170	PerCP-Fire 806	155536	Biolegend
XCR1	Spark UV387	148236	Biolegend
SIRPa	APC-Fire750	144030	Biolegend
CX3CR1	Spark Blue 574	285185	Biolegend
CD64	PE-Fire 744	161010	BD
PD1	RY586	753854	BD
FOXP3	e450	48-5773-82	Thermofisher

Validation

All antibodies were validated by the supplier and validation statements are available in the manufacturer's website. Additionally, functional experiments were reported in extended figures for murine T cell depletion antibodies provided in the manuscript.

Eukaryotic cell lines

Policy information about cell lines and Sex and Gender in Research

Cell line source(s)	AT3-OVA and D2A1 cell lines sourced from Prof. Phil Darcy and A/Prof Kara Britt respectively from Peter MacCallum Cancer Centre laboratory stocks, Melbourne, Australia
Authentication	Both cell lines were well established and published.
Mycoplasma contamination	Cell lines in this study were repetitively tested mycoplasma negative.
Commonly misidentified lines (See ICLAC register)	Cell lines in this study are not listed in the ILAC database.

Animals and other research organisms

Policy information about studies involving animals; ARRIVE guidelines recommended for reporting animal research, and Sex and Gender in Research

Laboratory animals	C57BL/6J wild type (wt) and BALB/c wt mice, RAG1-/-; RAG2-/-γc-/- and OT-I CD45.2 and gBT-I CD45.1/CD45.2.Mice were used between 7-8 weeks of age.
Wild animals	no wild animals were used in the study.
Reporting on sex	female mice
Field-collected samples	This study does not involve samples collected from the field
Ethics oversight	All animal experiments procedures conducted in this study were approved by the relevant Peter MacCallum Cancer Centre Animal Experimentation Ethics Committee or by The University of Melbourne Animal Ethics Committee and conducted in accordance with the National Health and Medical Research Council Australian Code of Practice for the Care and Use of Animals for Scientific Purposes.

Note that full information on the approval of the study protocol must also be provided in the manuscript.

Clinical data

Policy information about clinical studies

All manuscripts should comply with the ICMJE guidelines for publication of clinical research and a completed CONSORT checklist must be included with all submissions.

Clinical trial registration	We utilised immune scores and associated clinical information from the MyBrCa dataset obtained from the original publication that contain BC subtype, parity information and breastfeeding data were described Pan et al 2024. This was not a clinical trial
Study protocol	Clinical data previously reported in Pan ***et al*** 2024
Data collection	Extended MyBrCa demo table were provided in the supplemental table information in the current study and were previously described in Pan ***et al*** 2024.
Outcomes	Clinical data reported in Pan et al 2024. In this study we utilized report significantly higher tumoural immune content in “basal-like” TNBC in parous women overall, compared with the Nulliparous women who subsequently developed breast cancer and our parous (PB)-TRM gene signature was highly enriched with both parity and breastfeeding status, highlighting the specificity of the P-TRM signature to breast involution by parity, and the specific influence of lactation.

Plants

Seed stocks	not applicable
Novel plant genotypes	not applicable
Authentication	not applicable

Flow Cytometry

Plots

Confirm that:

☒ The axis labels state the marker and fluorochrome used (e.g. CD4-FITC).

☒ The axis scales are clearly visible. Include numbers along axes only for bottom left plot of group (a 'group' is an analysis of identical markers).

☒ All plots are contour plots with outliers or pseudocolor plots.

☒ A numerical value for number of cells or percentage (with statistics) is provided.

Methodology

Sample preparation	Human breast and Murine tissue samples were dissociated into single cell suspension was created using a modified published protocol Savas et al 2018. Adipose content were removed briefly from the mammary glands and the connective tissues were then finely diced into smaller fragments in RPMI1640 containing, 1 mg/ml collagenase type 4 and incubated for 30 minutes at 37C. Digested tissue fragments were teased through a 70um sieve, the sieve irrigated with neat PBS prior downstream analyses (Please refer further to respective tissue processing methods and resources table)
Instrument	BD Symphony A5 or LSR Fortessa X-20 (BD Biosciences, San Diego, CA, USA); 5-laser Cytek Aurora (Cytek Biosciences)
Software	FlowJo Version 10; OMIQ were used for FACS data interpretation and data presentation
Cell population abundance	Bulk RNA Seq, a total of 5x10e3 and blood 1x10e4 T cell fractions were FACS purified. Reanalysis of isolated CD8+ T cell following FACS were assessed for >90% purity of individual samples. total immune counts per gram were presented.
Gating strategy	Gating strategies including preliminary FSC/SSC gates of the starting population were provided **in Extended Data Figure 11 legends**

☒ Tick this box to confirm that a figure exemplifying the gating strategy is provided in the Supplementary Information.